Title	Influence of relative humidity on fracture toughness of rock: Implications for subcritical crack growth
Author(s)	Nara, Yoshitaka; Morimoto, Kazuya; Hiroyoshi, Naoki; Yoneda, Tetsuro; Kaneko, Katsuhiko; Benson, Philip M.
Citation	International Journal of Solids and Structures (2012), 49(18): 2471-2481
Issue Date	2012-09
URL	http://hdl.handle.net/2433/162014
Right	© 2012 Elsevier Ltd.
Type	Journal Article
Textversion	author

Influence of relative humidity on fracture toughness of rock: implications for subcritical crack growth

Yoshitaka Nara[1*], Kazuya Morimoto[2], Naoki Hiroyoshi[3], Tetsuro Yoneda[3], Katsuhiko Kaneko[3] and Philip M. Benson[4]

[1]*Department of Civil and Earth Resources Engineering, Graduate School of Engineering, Kyoto University, Kyoto daigaku-Katsura, Nishikyo-ku, Kyoto 615-8540, Japan.*

[2]*Department of Functional Material Science, Graduate School of Science and Engineering, Ehime University, 2-5 Bunkyo-cho, Matsuyama 790-8577, Japan.*

[3]*Division of Sustainable Resources Engineering, Faculty of Engineering, Hokkaido University, Kita 13 Nishi 8, Kita-ku, Sapporo, Hokkaido 060-8628, Japan.*

[4]*Geological Institute, Dept. Earth Sciences, Swiss Federal Institute of Technology, Sonneggstrasse 5, Zurich 8092, Switzerland*

*Corresponding author: Yoshitaka Nara

Address: Department of Civil and Earth Resources Engineering, Graduate School of Engineering, Kyoto University, Kyoto daigaku-Katsura, Nishikyo-ku, Kyoto 615-8540, Japan.

E-mail: nara.yoshitaka.2n@kyoto-u.ac.jp

Tel: +81 75 383 3211

Fax: +81 75 383 3213

Abstract

Information relating to the fracture toughness of geomaterials is critical to our understaing of tensile fracturing, and in particular in geological and rock engineering projects that are subjected to elevated moisture levels. In this study, we conducted a comprehensive set of fracture toughness tests on a suite of key rock types in air under different relative humidities and at constant temperature in order to investigate the influence of relative humidity on fracture toughness. Three sandstones and two igneous rocks were chosen for this purpose. We show that the value of fracture toughness decreases with increasing relative humidity. In addition, we find that the decrease in fracture toughness was more significant when the expansive clay such as smectite was included in rock. Since smectite is prone to expanding in the presence of water, the strength and thus crack growth resistance decrease when relative humidity is high. Therefore, we interpret the decreasing fracture toughness upon the degradation of expansive clays with increasing water content. It was also shown that the decrease of the fracture toughness with increasing humidity is less significant than the concomitant decrease in the measured value of the subcritical stress intensity factor. This was likely as a result of stress corrosion having little influence on the fracture toughness. We conclude that crack growth in rock is affected by humidity, and that clay content is an important contributing factor to changes in fracture toughness and subcritical stress intensity

factor.

Keywords: Fracture toughness, Subcritical crack growth, Double Torsion method, Relative humidity, Clay

1. Introduction

In order to ensure the stability of all solids and structures, studies of fracturing is essential. Several researchers have investigated the fracturing and failure of various solids (e.g., Atkinson, 1982, 1984; Atkinson and Meredith, 1987a, b; Biolzi and Labuz, 1993; Ayatollahi and Aliha, 2006; Ayatollahi and Torabi, 2010). Quantifying fracturing and faulting in rock masses is essential for our improved understanding in many geological phenomena such as volcanic eruptions and earthquakes. Kilburn and Voight (1998) reported that time-dependent fracturing of rock is related to the increase of seismicity detected prior to volcanic eruption. In addition, information relating to rock fracture is also important in the engineered environment (Jing, 2003). Such issues are of particular importance when dealing with longer term effects such as the integrity of subsurface structures like repositories for radioactive waste, caverns for the storage of liquid natural gas or liquid petroleum gas, and underground power plants. Chau and Shao (2006) reported that time-dependent crack growth in rock played an important role for the failure of rock panels on façade of buildings. Therefore, a number of investigations related to time-dependent fracturing in rock have been conducted.

Subcritical crack growth (SCG) is one of the main causes of time-dependent fracturing in rock (Atkinson, 1984; Atkinson and Meredith, 1987a; Dascalu et al., 2010), in addition it is well known that the presence of water in greatly affects SCG. According to the results of Waza

et al. (1980), Sano and Kudo (1992) and Nara et al. (2009), the crack-tip velocity in water saturated rock is much higher than that in air, and increased by 2-4 orders of magnitude. The water vapour pressure is also known to exert an influence, with Meredith and Atkinson (1985) and Nara and Kaneko (2005, 2006) both reporting and increase in crack velocity with increasing water vapour pressure. More recently, Nara et al. (2010, 2011a) reported that the crack velocity in air saturated rock increased with increasing relative humidity.

The influences of rock fabric on SCG have also been studied. Sano and Kudo (1992) and Nara and Kaneko (2006) reported that the crack velocity in granite is anisotropic due to the preferred orientation of microcracks. Nara et al. (2006) showed evidence that the geometry of the crack path became smoother for cracks propagating parallel to the Rift plane; the preferred plane of rupture caused by the preferred orientation of microcracks (Sano et al., 1992). Nara et al. (2011a) reported that the influence of the relative humidity on the crack velocity in rock was more significant when the rock included larger amount of clay minerals such as smectite and illite.

It has been clarified that SCG in rock is affected not only by the applied stress intensity factor but also by the environment and rock fabric. In order to better understand the fracturing in rock, it is therefore necessary to investigate the fracture toughness of rock. All rocks contain microcracks and microcavities (Sprunt and Brace, 1974; Nishiyama and Kusuda, 1994; Chen et al., 1999; Benson et al., 2006; Nara et al., 2011b). The influence of microcracks

on the fracture toughness has been investigated by numerous workers, for example Nasseri and Mohanty (2008) and Nasseri et al. (2005, 2006, 2007, 2009, 2011). According to these data results, the fracture toughness of granitic rocks is affected by the density and the length of microcracks distributed parallel to the crack propagation direction, which was manifested as anisotropy of fracture toughness (Nasseri et al., 2005, 2006, 2007, 2011). In addition, Nasseri et al. (2009) reported that the fracture toughness of thermally cracked Westerly granite decreases with increasing maximum temperature of thermal history and decreasing P-wave velocity.

The environmental influence upon fracture toughness has been studied to data on a wide variety of different rock types. Meredith and Atkinson (1985) reported the influence of temperature on the fracture toughness of Westerly granite and Black gabbro recording an increase in fracture toughness with increasing temperature up to 100 °C, as the advancing macrocrack tip encountered isolated microcracks unfavourably oriented with respect to the direction of macrocrack propagation. The thermally-induced microcracks thus behaved a barrier of macrocrack propagation for granite and gabbro up to 100 °C (Meredith and Atkinson, 1985). In contrast, Meredith and Atkinson reported that the fracture toughness of granite and gabbro decreased with increasing temperature when above 100 °C, interpreted due to the density and the length of microcracks in these rocks increasing due to thermal stress and resulting in an acceleration of macrocrack propagation. Utagawa et al. (1999) measured

the fracture toughness of Shin-komatsu andesite, Inada granite and Kimachi sandstone in both dry and wet conditions, and also reported data indicating a decrease in fracture toughness when liquid water was present at the crack tip. Wang et al. (2007) reported that the fracture toughness of clay decreased with increasing the water content. Al-Shayea et al. (2000) measured fracture toughness of a Saudi Arabian limestone exhibiting an increase in the fracture toughness with increasing the temperature up to 116 °C. Funatsu et al. (2004) investigated the fracture toughness of Kimachi sandstone and Tage tuff, in the former case measuring an almost constant fracture toughness up to 125 °C, and an increasing value beyond approximately 125 °C (Funatsu et al., 2004). Finally, Zuo et al. (2009) measured the fracture toughness of sandstone obtained at Pingdingshan (China), finding that the fracture toughness increased exponentially with elevated temperature in the range of 25 to 150 °C, and decreased exponentially from 150 to 300 °C.

In all of these studies, the key influences of microcracks, temperature, and presence (or not) of water have been investigated. However, the influence of the humidity on the fracture toughness of rock has yet to be fully explored. Fujii et al. (2011) reported that several large rock falls occurred in humid summer in Kushiro Coal Mine in Japan due to the weakening of rock by inflow of humid air. This report suggests that the investigation of the humidity effects on fracture toughness of rock is important for ensuring the stability of structures in a rock mass. In addition, it is important to compare the difference of the influence of environmental

conditions on the fracture toughness of rocks using a same fracture toughness testing protocol in order to best compare these key data across rock and environment parameters.

In this study, we have therefore investigated the influence of relative humidity on the fracture toughness of a suite of rocks (andesite, granite and three kinds of sandstone) using the same experimental protocols. In particular, we place special attention to measurements of the fracture toughness conducted in air by precisely controlling temperature and relative humidity and at constant temperature. We relate the change of the fracture toughness to the stress intensity factor for SCG.

2. Rock samples

All rock samples used in this study were manufactured from single blocks of Kumamoto andesite (KA), Oshima granite (OG), Berea sandstone (BS), Shirahama sandstone (SS) and Kushiro sandstone (KS). These were manufactured from the same blocks used in the previous studies (Nara and Kaneko, 2005, 2006; Nara et al., 2010, 2011a), where the petrological details of these rocks are provided.

In Table 1, P-wave velocities of rock samples under dry conditions are listed. P-wave velocities were measured by the ultrasonic transmission method in three orthogonal directions, axes-1, -2 and -3 in the order of increasing velocity. For sandstones and OG, axis-3 is normal to the bedding plane and Rift plane, respectively. The axis-1 of granite is normal to the Hardway plane. From Table 1, it is clear that OG has relatively high degree of anisotropy in its P-wave velocity, whereas the other rocks are relatively isotropic.

We therefore treat KA and the sandstone samples were treated as isotropic materials; OG was treated as an orthorhombic material based on previous data (Sano and Kudo, 1992; Nara and Kaneko, 2006). In this study, we found that cracks propagated normal to the Hardway plane, but parallel to the Rift plane in the OG sample. Therefore, the crack opening direction and propagation direction are defined as parallel to the axis-1 and axis-3 respectively.

3. Methods

3.1 Outline

In this study, the Double Torsion (DT) method was employed. The specimen and loading configuration of DT method is shown in Fig. 1, as well as the principal axes of symmetry for the orthorhombic OG. The loading direction shown in Fig. 1 is parallel to the principal axes if orthorhombic material is used.

In general, three different types of test can be conducted with the DT arrangement, each using different loading conditions: the constant load (CL) method (Kies and Clark, 1969), the constant displacement rate (CDR) method (Evans, 1972), and the load relaxation (RLX) method (Evans, 1972; Williams and Evans, 1973). We used the DT-CDR method in order to measure the fracture toughness and compare the results to those of SCG reported by Nara et al. (2010, 2011a).

In the DT-CDR method, the displacement rate of the loading points has to be kept constant during the experiment. To ensure this criterion is met, the displacement rate of the loading points should be large (Shyam and Lara-Curzio, 2006); this is especially important for applying this particular method to the calculation of fracture toughness. Finally, the maximum value of applied load at failure is used to calculate fracture toughness via the following

equations:

$$K_{\mathrm{Ic}} = P_{\max} w_{\mathrm{m}} \sqrt{\frac{3(1+\nu)}{W d^3 d_{\mathrm{n}}}} \tag{1}$$

$$K_{\mathrm{Ic}} = \left(\frac{3 {P_{\max}}^2 {w_{\mathrm{m}}}^2 s_{55}}{2 W d^3 d_{\mathrm{n}} (2 s_{33} ((s_{33} s_{11})^{1/2} + s_{13} + s_{55}/2))^{1/2}} \right)^{1/2} \tag{2}$$

where Eq. 1 is the equation for isotropic materials (Williams and Evans, 1973), and Eq. 2 is the equation for orthorhombic materials (Sano and Kudo, 1992) in the case that the crack opening direction and propagation direction are parallel to the axis-1 and axis-3 respectively. K_{Ic} is the fracture toughness, $P_{\max}$ is the maximum value of the applied load, w_{m} is the moment arm (18 mm for igneous rock and 23 mm for sandstones was used here), ν is Poisson's ratio of isotropic material, W is the width of the specimen, d is the thickness of the specimen, d_{n} is the reduced thickness of the specimen, and s_{ij} (i, j = 1, 3 or 5) is the elastic compliance of the orthorhombic material.

Crack velocity is estimated with the following equations:

$$\frac{\mathrm{d}a}{\mathrm{d}t} = \phi_{\mathrm{c}} \frac{W d^3 G}{3 {w_{\mathrm{m}}}^2 P_{\max}} \frac{\mathrm{d}y}{\mathrm{d}t} \tag{3}$$

$$\frac{\mathrm{d}a}{\mathrm{d}t} = \phi_{\mathrm{c}} \frac{2 d^3}{3 s_{55} w_{\mathrm{m}} P_{\max}} \frac{\mathrm{d}y}{\mathrm{d}t} \tag{4}$$

where Eq. 3 is the equation for isotropic materials (Williams and Evans, 1973) and Eq. 4 is the equation for orthorhombic materials (Sano and Kudo, 1992) in the case that the crack opening direction and propagation direction are parallel to the axis-1 and axis-3 respectively. da/dt is the crack velocity, G is the shear modulus, dy/dt is the displacement rate of the

loading points, and ϕ_c is a constant depending on the shape of the crack front. In this study, ϕ_c is set as 0.2 according to the observation of Williams and Evans (1973) for glass and Atkinson (1979a) for quartz.

In order to evaluate the fracture toughness and the crack velocity, we used the same values of the isotropic elastic moduli (G and v) for KA, BS, SS and KS as those used in the earlier work of Nara et al. (2010, 2011a), and the orthorhombic elastic moduli (s_{ij} (i, j = 1, 3 or 5)) as obtained by Nara and Kaneko (2006), respectively.

However, it is important to note that Eqs. 1-4 are approximate solutions based on a thin-plate assumption considering no thermal and hydro-mechanical phenomena (Williams and Evans, 1973; Sano and Kudo, 1992). In this case, according to experiments by Evans et al. (1974) and Atkinson (1979b), the thickness and width of the DT specimen have to satisfy the following condition:

$$12d \leq W \tag{5}$$

In addition, Ciccotti (2000) and Ciccotti et al. (2000a) derived a corrective factor relating the specimen compliance to the (non-linear) crack length in a DT specimen using a finite element analysis. Based on their results, a thicker specimen (W : d = 8 : 1) was shown to provide a robust solution (Ciccotti et al., 2000b, 2001). Sano (1988) went on to show that the proportional relation between the compliance and crack length in a DT specimen of glass and rocks is invariant, and therefore proved that the stress intensity factor of DT method is

independent of the crack length.

In Table 2, we summarise the width and thickness of DT specimens used in this study as well as the length L and reduced thickness d_n. It is clear that the values of the width and thickness satisfy the conditions suggested in previous studies.

3.2 Experimental apparatus and sample conditions

A schematic illustration of the apparatus used in this study is shown in Fig. 2. This apparatus consists of a speed-control (stepping) motor that drives the loading axis moving perpendicular to the DT specimen. The maximum velocity of the loading axis is 0.23 mm/s. This apparatus is housed in a temperature and humidity controlled room, ranging from 278-353 K and 40-90 %, respectively.

The applied load is measured by a load cell with an accuracy of ±0.04 N. Displacement of the load-points is measured by two linear variable displacement transformers (LVDTs) with the accuracy of ±0.5 μm.

In order to investigate the influence of the relative humidity, measurements were conducted under either (a), low humidity (289-295 K, 16-29 %), (b), intermediate humidity (293 K, 54-56 %) or (c), high humidity (293 K, 83-89 %) conditions. Unfortunately, however, it was

found to be impossible to achieve the low humidity conditions sought as well as controlling the temperature and the relative humidity because of a limitation of the controllable range. The low humidity condition was therefore achieved via the ambient (measured but not controlled) conditions found in the laboratory in winter.

3.3 Experimental procedure

Firstly, samples are pre-cracked in order to introduce a small starting crack into the specimen with the following method. Displacement is provided by the loading ram in 4 μm increments, each time pausing to allow the surface of the specimen to be observed using the digital microscope set under the specimen to measure crack length. We repeated this procedure until the crack length reached 25 mm for igneous rock samples and 30 mm for sandstone samples; these are the minimum length conditions required in which the stress intensity factor is independent of the crack length for a DT specimen as found by Trantina (1977):

$$0.55W < a < L - 0.65W \tag{6}$$

After the pre-cracking stage, the apparatus and specimen were exposed to the environmental condition of interest with the same temperature and relative humidity for

approximately 20 hours. Following this period, a fracture toughness measurement with DT-CDR method was performed using by applying a load at a displacement rate of 0.23 mm/s, which is the maximum rate of our apparatus, and after applying a small amount of pre-load around 10 N for igneous rock samples and less than 10 N for sandstone samples. Previous work has demonstrated an influence of measured stress intensity factor with loading rate when employing the DT-CDR method, with the use of a high displacement rates (above approximately 0.07 mm/s) mitigating this effect (Selçuk and Atkinson, 2000).

4. Results

Raw data from the 5 tests are presented in the form of load vs. time plots in Fig. 3. In each case the load increases rapidly over a period of 2-7 seconds. In the case of Kumamoto andesite (KA), the force increases very rapidly over just 2 seconds reaching a peak of ~75N (Fig. 3a). For Oshima granite (Fig. 3b) the rise in force is slightly slower, reaching ~80N in ~3s. The sandstone experiments, there is a noticeably slower rise to peak force of ~4.5s, ~7s, and ~5s for BS, SS and KS respectively, and a lower peak force at failure of 17N, 22N, and 41N respectively, reflecting the different elastic properties of the materials in question. The value of force at peak stress is then used to calculate the fracture toughness via Eq. 1 or, in the case of OG, Eq. 2.

These fracture toughness data for each rock type are plotted in Fig. 4, as a function of relative humidity. In all cases a decrease in K_{IC} with increasing relative humidity is measured. For KA and OG, a large scatter is evident in the data, with successive measurements also showing some variation. Nonetheless a statistically significant decrease in fracture toughness is measured (Fig 4a. and Fig. 4b). For three sandstones, the reproducibility of K_{IC} measurements is excellent, with tight clustering of the repeated data points. A very clear decrease in fracture toughness is measured for each sandstone (Figs. 4c, d, e). In addition the rate of decrease of K_{IC} as relative humidity varies from 0-100% also increases from BS (0.1

$MN/m^{3/2}$), through SS (0.45 $MN/m^{3/2}$) to KS, which shows the greatest decrease of 0.5 $MN/m^{3/2}$ over the same range, likely related to the different rock microstructures involved.

In Table 3, we summarize the results of the fracture toughness measurements, showing values of average and standard deviation from each of 2-3 measurements at each relative humidity and each rocky type. It is clear that the average fracture toughness tends to be lower at elevated relative humidity. The crack velocity for fracture toughness measurement was 10^{-1}-10^{-2} m/s in all measurements.

5. Discussion

5.1 The Double Torsion method as a fracture toughness measurement

As the DT method is not traditionally a standard method for fracture toughness measurement of rock (International Society for Rock Mechanics, 1988, 1995), it is instructive to explore the reliability of data obtained by this method for fracture toughness.

The DT method has been used for the measurement of subcritical crack growth. For the deformation of glass in air, SCG is divided into three key regions with respect to the difference in mechanism which controls the crack velocity (Fig. 5). In Region-I, the crack velocity is controlled by the rate of stress corrosion which is the chemical reaction between the siloxane bond and a reactive agent (water in this case) at the crack tip under tension (Anderson and Grew, 1977). In Region-II, the crack velocity is controlled by the rate of transport of the reactive agent to the crack tip (Lawn, 1975). In Region-III, the crack propagation is relatively insensitive to the chemical environment and occurs mechanically (Wiederhorn et al., 1974). This is illustrated in Fig. 5, showing the classic tri-modal behaviour of the K_I-da/dt relation (between the crack velocity and stress intensity factor) for SCG (after Atkinson and Meredith (1987a)) and the K_I-da/dt relation of soda-lime glass obtained experimentally. K_I-da/dt relations, shown in Fig. 5b, were obtained by the DT-RLX method. It

is therefore possible to estimate the fracture toughness if three regions are observed clearly as shown in Fig. 5b.

In the case of rocks used in this study, however, it was not possible to observe the three regions of SCG (Nara and Kaneko, 2005, 2006; Nara et al., 2010, 2011a). Often, only Region-I behaviour is observed for rock (Atkinson, 1984; Atkinson and Meredith, 1987a). Therefore, it is necessary to use an alternative approach to measure the fracture toughness of rock. In this study, we chose the DT-CDR method as a solution to this requirement, applying it to the measurement of fracture toughness via Eqs. 1 and 2. This approach has been previously applied by Atkinson (1979b), Meredith (1983) and Meredith and Atkinson (1985) who applied the DT-CDR method using displacement rates of approximately 20 mm/min (around 0.33 mm/s) (Atkinson, 1979b; Meredith, 1983) and 10 mm/min (around 0.17 mm/s) (Meredith, 1983; Meredith and Atkinson, 1985), respectively. These displacement rates are higher than that mentioned by Selçuk and Atkinson (2000) (0.07 mm/s, see Section 3.3). Meredith (1983) reported that the fracture toughness values obtained by DT-CDR method agreed well with those obtained by the short-rod method which is the standard method for fracture toughness measurement of rock (International Society for Rock Mechanics, 1988).

Even though the values of the crack velocity were not provided in Atkinson (1979b), Meredith (1983) and Meredith and Atkinson (1985), it is possible to calculate the crack velocity using Eqs. 1 and 3 with the specimen size, elastic constants, displacement rate and

the fracture toughness. Here, we evaluate the crack velocity for Tennessee sandstone (Atkinson, 1979b) and Westerly granite (Meredith and Atkinson, 1985). For Tennessee sandstone, the displacement rate and the fracture toughness are 0.33 mm/s and 0.45 $MN/m^{3/2}$, respectively (Atkinson, 1979b); for Westerly granite, the displacement rate and the fracture toughness are 0.17 mm/s and 1.8 $MN/m^{3/2}$, respectively (Meredith and Atkinson, 1985). A crack velocity of 6×10^{-2} m/s is calculated for both Tennessee sandstone and Westerly granite.

Therefore, even though the crack velocities in this study (see Table 3) were calculated from experiments made at a higher displacement rate (0.23 mm/s), they agree well with the calculated velocity above. Furthermore, this velocity is likely high enough to assume that the crack velocity corresponds to the fracture toughness of rock. We thus consider that the measurement with DT-CDR method in this study provided the appropriate value of the fracture toughness of rock.

5.2 Influence of humidity on stress intensity factor

As shown in Fig. 4, the fracture toughness undergoes a noticeable decrease with increasing relative humidity. Whilst the decreases were very prominent for SS and KS, the general decrease was measured for all rock types studied.

Although a detailed microstructural and compositional study is beyond the scope of this paper, it is likely that the different compositions in the rocks chosen have a significant effect on the change of K_{Ic}. Nara et al. (2010) suggested that for igneous rock types the increase of the humidity also brings about an increase in the presence of condensed water by the capillary condensation of water vapour around the crack tips, and thus induces a reduction in the crack growth resistance. It is likely that other rock types that contain few clay minerals (such as Berea sandstone) would be similarly affected (Nara et al., 2011a). The aperture of the crack close to the crack tip is very small. It is therefore possible that the water vapour turns to liquid water by capillary condensation in this zone, and that the crack path close to the crack tip is therefore immersed in liquid water. Since suction therefore occurs between the crack planes by liquid bridging if the crack is immersed in a liquid (Thomson, 1871), compressive stress acts around the crack tip. This suction will decrease with increasing radius of curvature of the condensed liquid. Increase in relative humidity will lead to an increase in the volume of condensed water present. In this case, the radius of curvature of the liquid water will increase as the aperture of the crack increases. The Young-Laplace equation describes the capillary pressure difference sustained across the interface between two static fluids such as water and air. By using this equation, it is possible to approximate the compressive stress around the crack tip. If the aperture of the crack is $2r$, the Young-Laplace equation is expressed as follows (Schulze, 1984):

$$P_c = \frac{\gamma_s}{r} \tag{7}$$

where P_c is the pressure due to the capillary condensation, that is, the compressive stress around the crack tip, and γ_s is the surface tension of water, which is 73×10^{-3}N/m. In the images of the crack paths in granite obtained with the Electron Prove Micro Analyzer by Nara et al. (2006), the least aperture of the crack is less than 10 nm. For example, assuming that r = 5 or 10 [nm], the compressive stress around the crack tip is 14.6 MPa or 7.3 MPa, respectively. These values are similar to the tensile strength of rocks. If the value of r is smaller than those above, the compressive stress around the crack tip increases. Considering the value of the compressive stress extimated above, the influence of the compressive stress around the crack tip due to the capillary condensation should be significant.

For sandstones containing smectite, it has additionally been hypothesised that the increase of humidity causes a weakening of smectite, resulting in decreased crack growth resistance (Nara et al., 2011a). Finally, we suggest that increased internal tensile stresses occur due to the expansion of smectite at elevated humidity levels, resulting in the water content of smectite also increasing.

The similar tendency was observed for SCG (Nara et al., 2010, 2011a), whereby the stress intensity factor for the same crack velocity also decreased with increasing relative humidity. It is therefore important to accurately compare and contrast the changes in fracture toughness to that of the stress intensity factor for the same response as measured in SCG. In Fig. 6, this

exercise has been performed, illustrating that the relation between fracture toughness and stress intensity factor is highly dynamic; to better visualise this relationship, the changes have been normalized by the data collected under the lowest humidity conditions to better show the effect of the increase in relative humidity. In this figure, solid symbols indicate the fracture toughness (K_{Ic}) and open symbols indicate the stress intensity factor for SCG at the crack velocity of 10^{-5} m/s ($K_I(10^{-5})$) obtained by Nara et al. (2010, 2011a).

From Fig. 6, it is clear that the decrease of K_{Ic} and $K_I(10^{-5})$ for SS and KS are more significant than those of KA, OG and BS. It is already established that SS and KS contain smectite. Furthermore, it has previously been shown that if the content of water in smectite increases, the basal spacing increases (Sato et al., 1992), and the strength of sandstone containing smectite decreases (Young et al., 2009). According to the observation of Sato et al. (1992), the basal spacing of smectite at 90% of the relative humidity was around 1.2 ~ 1.6 times larger than those at 20% of relative humidity. Since the water content of rock increases under high humidity conditions, we hypothesise that the bulk of the decrease in crack growth resistance is due to the presence of smectite.

Finally, we note that the decrease of K_{Ic} tends to be smaller than that of $K_I(10^{-5})$ for all rocks measured (Fig. 6). During SCG, stress corrosion is one of the main mechanisms (Anderson and Grew, 1977; Atkinson, 1984; Atkinson and Meredith, 1987a). Conversely, stress corrosion has few significant effects on the crack propagation at the crack velocity

occurring during the fracture toughness measurements. Therefore, we hypothesise that $K_I(10^{-5})$ decreased more obviously than K_{Ic} because of the influence of stress corrosion.

5.3 K_I-da/dt relation for subcritical crack growth normalized by K_{Ic}

Generally, the K_I-da/dt relation for SCG is expressed as follows (Charles, 1958; Wiederhorn and Bolz, 1970):

$$\frac{da}{dt} = AK_I^{\,n} \exp\left(\frac{-E^{\ddagger}}{RT}\right) \tag{8}$$

$$\frac{da}{dt} = v_0 \exp\left(\frac{-E^{\ddagger} + bK_I}{RT}\right) \tag{9}$$

where $E^{\ddagger}$ is the stress-free activation energy, R is the gas constant, T is the absolute temperature, and others are constants determined experimentally. Especially, n is called subcritical crack growth index (Atkinson, 1984; Atkinson and Meredith, 1987a).

Nara et al. (2010, 2011a) considered that the stress-free activation energy was affected by the change of the humidity due to the effect of condensed water around the crack tip by capillary condensation. If chemical reactions, such as stress corrosion, do not act during the crack propagation, the energy required for the crack propagation should be equal or greater than the fracture toughness. Therefore, the stress-free activation energy is directly related to the fracture toughness. Based on this theory, it is likely that K_I-da/dt relations for SCG

obtained under different environmental conditions should agree with each other if they are normalized by the fracture toughness K_{Ic}. This normalisation process is presented in Fig. 7 (K_I/K_{Ic}-da/dt). In the case of KA, OG and BS, we note that the K_I/K_{Ic}-da/dt relations are distributed in similar positions of K_I/K_{Ic} even though each relation was obtained under different humidity conditions. The K_I/K_{Ic}-da/dt relation for KA is in particularly good agreement. On the other hand, the agreement of K_I/K_{Ic}-da/dt relations for SS and KS are poor. For SS, the K_I/K_{Ic}-da/dt relation obtained under the high humidity conditions is shown in the region of lower stress intensity factor; likewise in the case of KS, the K_I/K_{Ic}-da/dt relationship obtained under the intermediate and high humidity conditions are also shown in this region.

It is therefore clarified that the K_I/K_{Ic}-da/dt relations provide evidence that rocks containing only a small proportion of clay minerals under different humidities are broadly in agreement in terms of their stress intensity factor. In addition, we analyse the proportion of clays contained in rock, noting that this affects the disagreement of K_I/K_{Ic}-da/dt relations under different humidities. Since the reason of disagreement is currently not fully understood, additional experiments on tensile fracturing in rocks of differing, well characterised, clay contents and under different humidities will be necessary, and is the subject of future research.

In Eqs. 8 and 9, it would be necessary to include some components considering the mechanical influences such as the repulsive force due to the capillary condensation and the fracture resistance change in expansive clays into account. If we can consider the mechanical

influences of the relative humidity in the evaluation of the crack velocity and stress intensity factor, better understanding of the fracturing of rock is possible, and we can ensure the stability of structures in a rock mass. In order to complete this work, we need more results in other rock types. This will also be the future subject.

6. Conclusions

We have investigated the influence of the relative humidity on the fracture toughness of a suite of five rocks using the Double Torsion method. We find that the fracture toughness of rocks decreases in the presence of high relative humidity. This tendency was much more obvious when the rocks included expansive clays such as smectite. The decrease of the fracture toughness with increasing humidity was, however, smaller than that of the stress intensity factor for subcritical crack growth, because stress corrosion has little influence on the fracturing at the fracture toughness.

This study reveals a significant influence of the relative humidity and the existence of expansive clays in porous rocks. As a consequence, the resistance of fracturing in rock decreases when the relative humidity is high; this has application to a wide range of applied geoscience issues such as the deep geological disposal of radioactive waste requiring a long terms natural rock cavern. For retarding fracturing in rock and making sure the stability of structures in a rock mass, it is thus effective to control the relative humidity of surrounding environment.

Acknowledgement

The authors appreciate Prof. Yoshiaki Fujii at Hokkaido University and Kushiro Coalmine Co. LTD. for donating the sample of Kushiro sandstone.

References

Al-Shayea, N.A., Khan, K., Abduljauwad, S.N., 2000. Effects of confining pressure and temperature on mixed-mode (I-II) fracture toughness of a limestone rock. Int. J. Rock Mech. Min. Sci. 37, 629-643.

Anderson, O.L., Grew, P.C., 1977. Stress corrosion theory of crack propagation with applications to geophysics. Rev. Geophys. Space Phys. 15, 77-104.

Atkinson, B.K., 1979a. A fracture mechanics study of subcritical tensile cracking of quartz in wet environments. Pure Appl. Geophys. 117, 1011-1024.

Atkinson, B.K., 1979b. Fracture toughness of Tennessee sandstone and Carrara marble using the double torsion testing method. Int. J. Rock Mech. Min. Sci. & Geomech. Abstr. 16, 49-53.

Atkinson, B.K., 1982. Subcritical crack-propagation in rocks – theory, experimental results and applications. J. Struct. Geol. 4, 41-56.

Atkinson, B.K., 1984. Subcritical crack growth in geological materials. J. Geophys. Res. 89, 4077-4114.

Atkinson, B.K., Meredith, P.G., 1987a. The theory of subcritical crack growth with applications to minerals and rocks. In: Atkinson, B.K. (Ed.), Fracture Mechanics of Rock, Academic Press, London, pp. 111-166.

Atkinson, B.K., Meredith, P.G., 1987b. Experimental fracture mechanics data for rocks and minerals. In: Atkinson, B.K. (Ed.), Fracture Mechanics of Rock, Academic Press, London, pp. 477-525.

Ayatollahi, M.R., Aliha, M.R.M., 2006. On determination of mode II fracture toughness using semi-circular bend specimen. Int. J. Solids Struct. 43, 5217-5227.

Ayatollahi, M.R., Torabi, A.R. 2010. Determination of mode II fracture toughness for U-shaped notches using Brazilian disc specimen. Int. J. Solids Struct. 47, 454-465.

Benson, P.M., Meredith, P.G., Schubnel, A., 2006. Role of void space geometry in permeability evolution in crustal rocks at elevated pressure. J. Geophys. Res. 111, B12203, doi:10.1029/2006JB004309.

Biolzi, L., Labuz, J.F., 1993. Global instability and bifurcation in beams composed of rock-like materials. Int. J. Solids Struct. 30, 359-370.

Charles, R.J., 1958. Static fatigue of glass II. J. Appl. Phys. 29, 1554-1560.

Chau, K.T., Shao, J.F., 2006. Subcritical crack growth of edge and center cracks in façade rock panels subject to periodic surface temperature variations. Int. J. Solids Struct. 43, 807-827.

Chen, Y., Nishiyama, T., Kusuda, H., Kita, H., Sato, T., 1999. Correlation between microcrack distribution patterns and granitic rock splitting planes. Int. J. Rock Mech. Min. Sci. 36, 535-541.

Ciccotti, M., 2000. Realistic finite-element method for double-torsion loading configuration. J. Am. Ceram. Soc. 83, 2737-2744.

Ciccotti, M., Gonzato. G., Mulargia, F., 2000a. The double torsion loading configuration for fracture propagation: an improved methodology for the load-relaxation at constant displacement. Int. J. Rock Mech. Min. Sci. 37, 1103-1113.

Ciccotti, M., Negri, N., Sassi, L., Gonzato, G., Mulargia, F., 2000b. Elastic and fracture parameters of Etna, Stromboli, and Vulcano lava rocks. J. Volcanol. Geother. Res. 98, 209-217.

Ciccotti, M., Negri, N., Gonzato, G., Mulargia, F., 2001. Practical application of an improved methodology for the double torsion load relaxation method. Int. J. Rock Mech. Min. Sci. 38, 569-576.

Dascalu, C., François, B., Keita, O. 2010. A two-scale model for subcritical damage propagation. Int. J. Solids Struct., 47, 493-502.

Evans, A.G., 1972. A method for evaluating the time-dependent failure characteristics of brittle materials – and its application to polycrystalline alumina. J. Mater. Sci. 7, 1137-1146.

Evans, A.G., Linzer, M., Russell, L.R., 1974. Acoustic emission and crack propagation in polycrystalline alumina. Mater. Sci. Eng. 15, 253-261.

Fujii, Y., Ishijima, Y., Ichihara, Y., Kiyama, T., Kumakura, S., Takada, M., Sugawara, T.,

Narita, T., Kodama, J., Sawada, M., Nakata, E. 2011. Mechanical properties of abandoned and closed roadways in the Kushiro Coal Mine, Japan. Int. J. Rock Mech. Min. Sci. 48, 585-596.

Funatsu, T., Seto, M., Shimada, H., Matsui, K., Kuruppu, M., 2004. Combined effects of increasing temperature and confining pressure on the fracture toughness of clay bearing rocks. Int. J. Rock Mech. Min. Sci. 41, 927-938.

International Society for Rock Mechanics, 1988. Suggested methods for the fracture toughness of rock. Int. J. Rock Mech. Min. Sci. 25, 71-96.

International Society for Rock Mechanics, 1995. Suggested method for determining Mode I fracture toughness using Cracked Chevron Notched Brazilian Disc (CCNBD) specimen. Int. J. Rock Mech. Min. Sci. 32, 57-64.

Jing, L., 2003. A review of techniques, advances and outstanding issues in numerical modelling for rock mechanics and rock engineering. Int. J. Rock Mech. Min. Sci. 40, 283-353.

Kies, J.A., Clark, A.B.J., 1969. Fracture propagation rates and times to fail following proof stress in bulk glass. In: Platt, P.L. (Ed.), Fracture 1969, Chapman and Hall, London, pp. 483-491.

Kilburn, C.R.J., Voight, B., 1998. Slow rock fracture as eruption precursor at Soufriere Hills volcano, Montserrat. Geophys. Res. Lett. 25, 3665-3668.

Lawn, B.R., 1975. An atomistic model of kinetic crack growth in brittle solids. J. Mater. Sci., 10, 469-480.

Meredith, P.G., 1983. A fracture mechanics study of experimentally deformed crustal rocks. Ph.D. Thesis, University of London.

Meredith, P.G., Atkinson, B.K., 1985. Fracture toughness and subcritical crack growth during high-temperature tensile deformation of Westerly granite and Black gabbro. Phys. Earth Planet. Inter. 39, 33-51.

Nara, Y., Kaneko, K., 2005. Study of subcritical crack growth in andesite using the Double Torsion test. Int. J. Rock Mech. Min. Sci. 42, 521-530.

Nara, Y., Kaneko, K., 2006. Sub-critical crack growth in anisotropic rock. Int. J. Rock Mech. Min. Sci. 43, 437-453.

Nara, Y., Koike, K., Yoneda, T., Kaneko, K., 2006. Relation between subcritical crack growth behavior and crack paths in granite. Int. J. Rock Mech. Min. Sci. 43, 1256-1261.

Nara, Y., Takada, M., Igarashi, T., Hiroyoshi, N., Kaneko, K., 2009. Subcritical crack growth in rocks in an aqueous environment. Explor. Geophys. 40, 163-171.

Nara, Y., Hiroyoshi, N., Yoneda, T., Kaneko, K., 2010. Effect of temperature and relative humidity on subcritical crack growth in igneous rock. Int. J. Rock Mech. Min. Sci. 47, 640-646.

Nara, Y., Morimoto, K., Yoneda, T., Hiroyoshi, N., Kaneko, K., 2011a. Effects of humidity

and temperature on subcritical crack growth in sandstone. Int. J. Solids Struct. 48, 1130-1140.

Nara, Y., Kato, H., Yoneda, T., Kaneko, K., 2011b. Determination of three-dimensional microcrack distribution and principal axes for granite using a polyhedral specimen. Int. J. Rock Mech. Min. Sci. 48, 316-335.

Nasseri, M.H.B., Mohanty, B., 2008. Fracture toughness anisotropy in granitic rocks. Int. J. Rock Mech. Min. Sci., 45, 167-193.

Nasseri, M.H.B., Mohanty, B., Robin, P.-Y.F., 2005. Characterization of microstructures and fracture toughness in five granitic rocks. Int. J. Rock Mech. Min. Sci., 42, 450-460.

Nasseri, M.H.B., Mohanty, B., Young, R.P., 2006. Fracture toughness measurements and acoustic emission activity in brittle rocks. Pure Appl. Geophys. 163, 917-945.

Nasseri, M.H.B., Schubnel, A., Young, R.P., 2007. Coupled evolutions of fracture toughness and elastic wave velocities at high crack density in thermally treated Westerly granite. Int. J. Rock Mech. Min. Sci. 44, 601-616.

Nasseri, M.H.B., Schubnel, A., Benson, P.M., Young, R.P., 2009. Common evolution of mechanical and transport properties in thermally cracked westerly granite at elevated hydrostatic pressure. Pure Appl. Geophys. 166, 927-948.

Nasseri, M.H.B., Rezanezhad, F., Young, R.P., 2011. Analysis of fracture damage zone in anisotropic granitic rock using 3D X-ray CT scanning techniques. Int. J. Fract. 168, 1-13.

Nishiyama, T., Kusuda, H., 1994. Identification of pore spaces and microcracks using fluorescent resins. Int. J. Rock Mech. Min. Sci. & Geomech. Abstr. 31, 369-375.

Sano, O., 1988. A revision of the double-torsion technique for brittle materials. J. Mater. Sci. 23, 2505-2511.

Sano, O., Kudo, Y., 1992. Relation of fracture resistance to fabric for granitic rocks. Pure Appl. Geophys. 138, 657-677.

Sano, O., Kudo, Y., Mizuta, Y., 1992. Experimental determination of elastic constants of Oshima granite, Barre granite, and Chelmsford granite. J. Geophys. Res. 97, 3367-3379.

Sato, T., Watanabe, T., Otsuka, R., 1992. Effects of layer charge, charge location, and energy change on expansion properties of dioctahedral smectites. Clay Clay Min. 40, 103-113.

Schulze, H.J., 1984. Physico-chemical elementary processes in flotation. Amsterdam, Elsevier.

Selçuk, A., Atkinson, A., 2000. Strength and toughness of tape-cast yttria-stabilized zirconia. J. Am. Ceram Soc. 83, 2029-2035.

Shyam, A., Lara-Curzio, E., 2006. The double-torsion testing technique for determination of fracture toughness and slow crack growth behaviour of materials: a review. J. Mater. Sci. 41, 4093-4104.

Sprunt, E.S., Brace, W.F., 1974. Direct observation of microcavities in crystalline rocks. Int. J. Rock Mech. Min. Sci. & Geomech. Abstr. 11, 139-150.

Thomson, W. 1871. On equilibrium of vapour at a curved surface of liquid. Philos. Mag. 42, 448-452.

Trantina, G.G., 1977. Stress analysis of the double-torsion specimen. J. Am. Ceram. Soc. 60, 338-341.

Utagawa, M., Seto, M., Kosugi, M., Katsuyama, K., Matsui, K., 1999. The evaluation of fracture toughness of rock in wet and chemical condition. Proceedings of ’99 Japan-Korea Joint Symposium on Rock Engineering. pp. 573-578.

Wang, J.G., Zhu, J.G., Chiu, C.F., Zhang, H., 2007. Experimental study on fracture toughness and tensile strength of a clay. Eng. Geol. 94, 65-75.

Waza, T., Kurita, K., Mizutani, H., 1980. The effect of water on the subcritical crack growth in silicate rocks. Tectonophys. 67, 25-34.

Wiederhorn, S.M., Bolz, L.H., 1970. Stress Corrosion and Static Fatigue of Glass. J. Am. Ceram. Soc. 53, 543-548.

Wiederhorn, S.M., Johnson, H., Diness, A.M., Heuer, A.H., 1974. Fracture of glass in vacuum. J. Am. Ceram. Soc. 57, 336-341.

Williams, D.P., Evans, A.G., 1973. A simple method for studying slow crack growth. J. Test. Eval. 1, 264-270.

Young, R.W., Wray, R.A.L., Young, A.R.M., 2009. Sandstone Landforms. Cambridge University Press, Cambridge.

Zuo, J.P., Xie, H.P., Zhou, H.W., 2009. Experimental determination of coupled thermal-mechanical effects on fracture toughness of sandstone. J. Test. Eval. 37, doi:10.1520/JTE101542.

Figure captions

Fig. 1 Schematic illustration of Double Torsion specimen and loading configuration. The loading forces are shown by four thick arrows.

Fig. 2 Experimental apparatus for fracture toughness measurement.

Fig. 3 Temporal changes of applied load for constant displacement rate experiments of Double Torsion method. (a): Kumamoto andesite, (b): Oshima granite, (c): Berea sandstone, (d): Shirahama sandstone, (e): Kushiro sandstone.

Fig. 4 Relations between fracture toughness and relative humidity. (a): Kumamoto andesite, (b): Oshima granite, (c): Berea sandstone, (d): Shirahama sandstone, (e): Kushiro sandstone.

Fig. 5 Relations between crack velocity and stress intensity factor for subcritical crack growth in glass in air. K_0 is the subcritical crack growth limit. (a): Schematic diagram (after Atkinson and Meredith (1987a)), (b): Relations obtained experimentally for soda-lime glass.

Fig. 6 Changes of fracture toughness and stress intensity factor for subcritical crack growth with increasing relative humidity. The values of stress intensity factors and relative humidity are normalized by the values for the low humidity condition.

Fig. 7 Relations between crack velocity and stress intensity factor normalized by fracture toughness. (a): Kumamoto andesite, (b): Oshima granite, (c): Berea sandstone, (d): Shirahama sandstone, (e): Kushiro sandstone.

Tables

Table 1 P-wave velocities in rock samples in dry condition.

Rock samples	P-wave velocities [km/s]		
	axis-1	axis-2	axis-3
Kumamoto andesite	4.8	4.8	4.8
Oshima granite	4.9	4.6	4.5
Berea sandstone	2.3	2.3	2.2
Shirahama sandstone	2.9	2.8	2.6
Kushiro sandstone	2.9	2.7	2.7

Table 2 Size of Double Torsion specimen.

Rock samples	Width [mm]	Thickness [mm]	Length [mm]	Reduced thickness [mm]
Kumamoto andesite	45.0	3.0	150	2.0
Oshima granite	45.0	3.0	150-170	2.0
Berea sandstone	55.0	3.5	145	2.5
Shirahama sandstone	55.0	3.5	145	2.5
Kushiro sandstone	55.0	4.0	145	3.0

Table 3 Summary of the results of fracture toughness measurements.

Rock samples	Temperature [K]	Relative humidity [%]	Fracture toughness [$MN/m^{3/2}$]	Crack velocity [m/s]
Kumamoto andesite	293	85-87	1.66±0.05	$(4.92±0.13)×10^{-2}$
	293	54	1.83±0.21	$(4.48±0.51)×10^{-2}$
	289-290	22-23	1.91±0.03	$(4.25±0.07)×10^{-2}$
Oshima granite	293	83-85	2.06±0.06	$(1.22±0.11)×10^{-2}$
	293-294	27-29	2.14±0.09	$(1.14±0.04)×10^{-2}$
Berea sandstone	293	86-88	0.30±0.01	$(6.91±0.23)×10^{-2}$
	293	54-55	0.33±0.01	$(6.35±0.08)×10^{-2}$
	293	16-17	0.36±0.01	$(5.67±0.06)×10^{-2}$
Shirahama sandstone	293	88-89	0.39±0.02	$(3.90±0.20)×10^{-2}$
	293	54-56	0.48±0.02	$(3.17±0.14)×10^{-2}$
	293-294	16	0.73±0.01	$(2.08±0.03)×10^{-2}$
Kushiro sandstone	293	84-86	0.60±0.02	$(1.61±0.06)×10^{-2}$
	293	55-56	0.75±0.02	$(1.28±0.03)×10^{-2}$
	292-295	23-27	0.89±0.07	$(1.07±0.08)×10^{-2}$

Figure1

Click here to download high resolution image

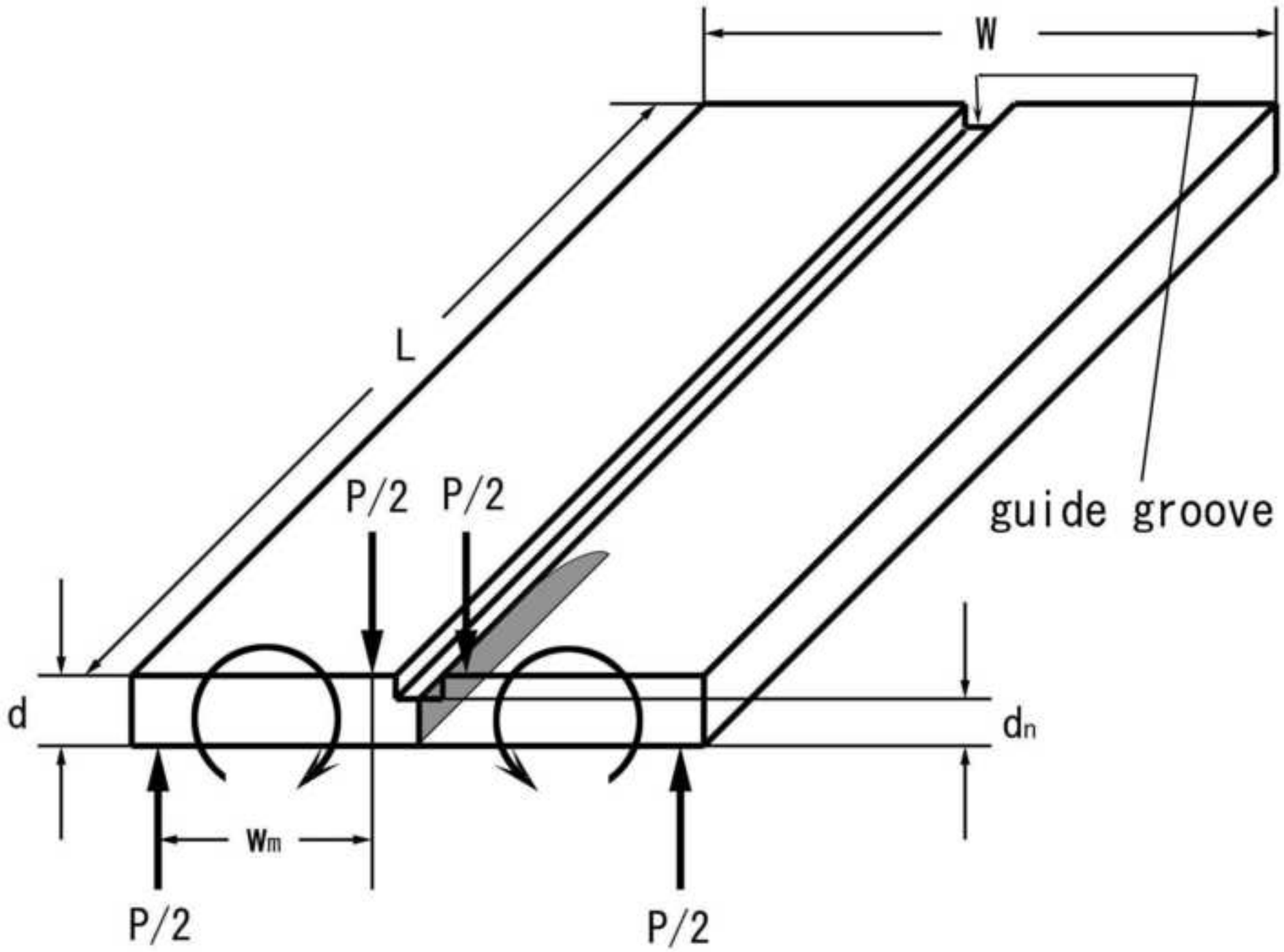

Figure2

Click here to download high resolution image

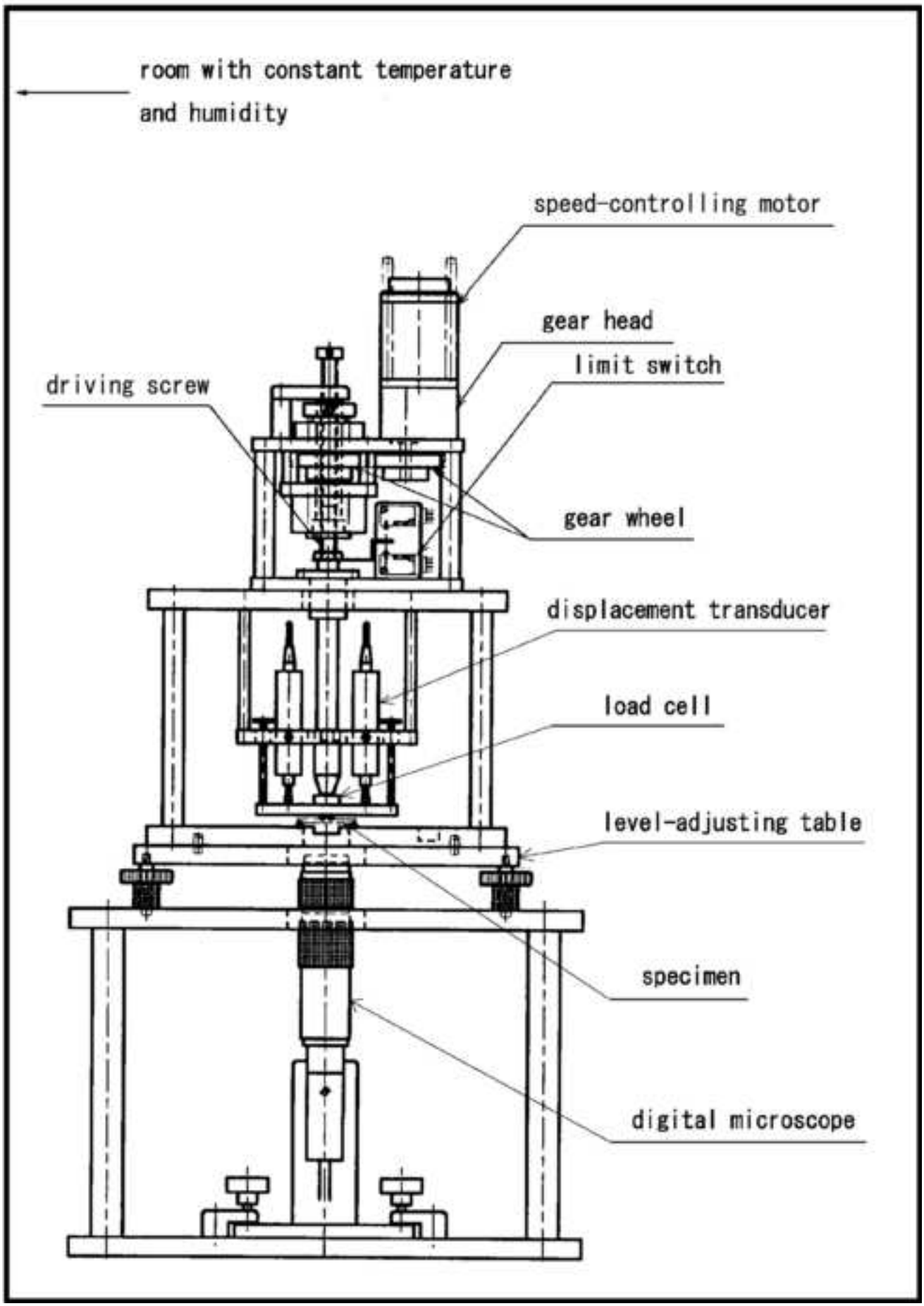

Figure3a
Click here to download high resolution image

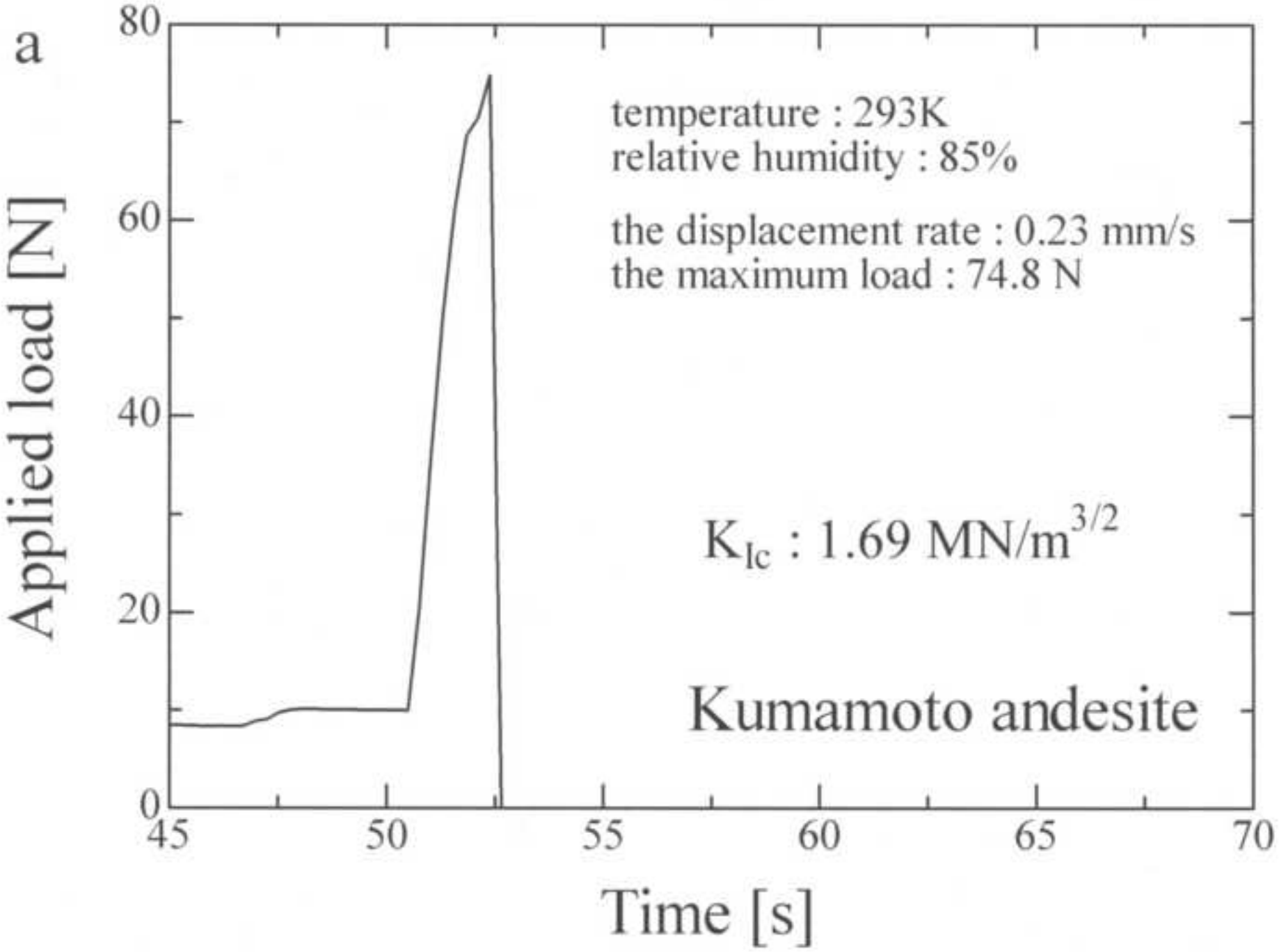

Figure3b
Click here to download high resolution image

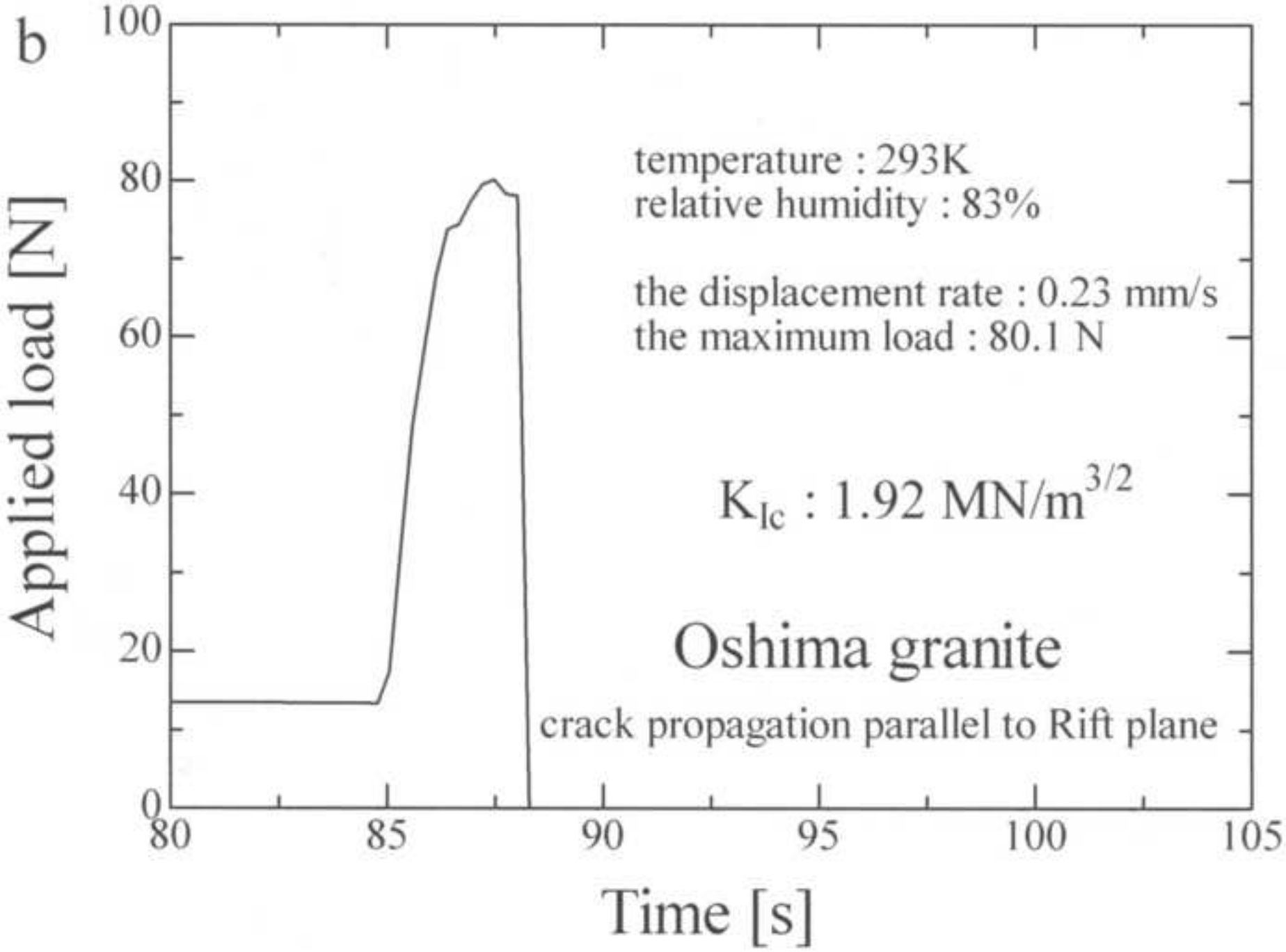

Figure3c
Click here to download high resolution image

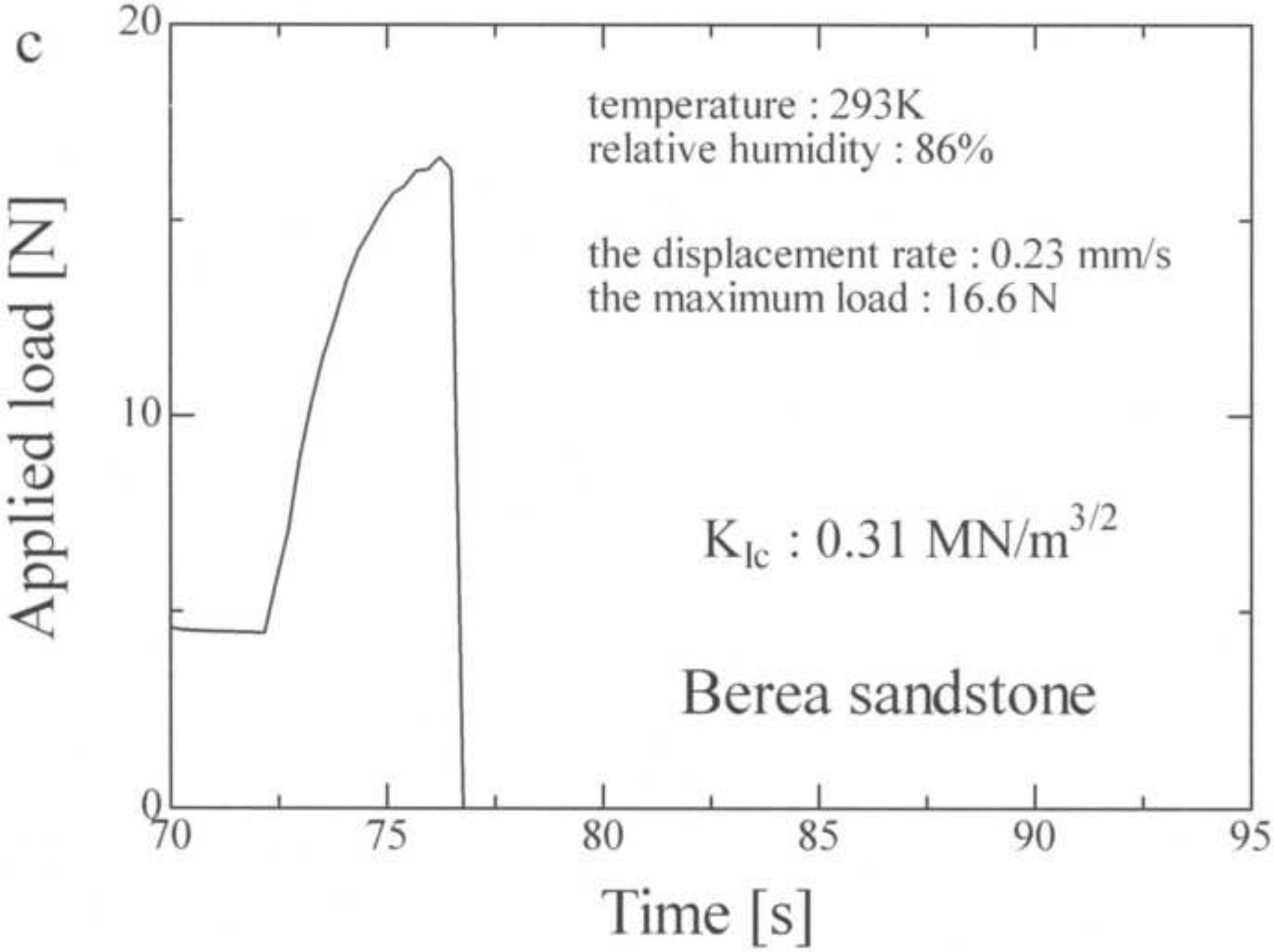

Figure3d
Click here to download high resolution image

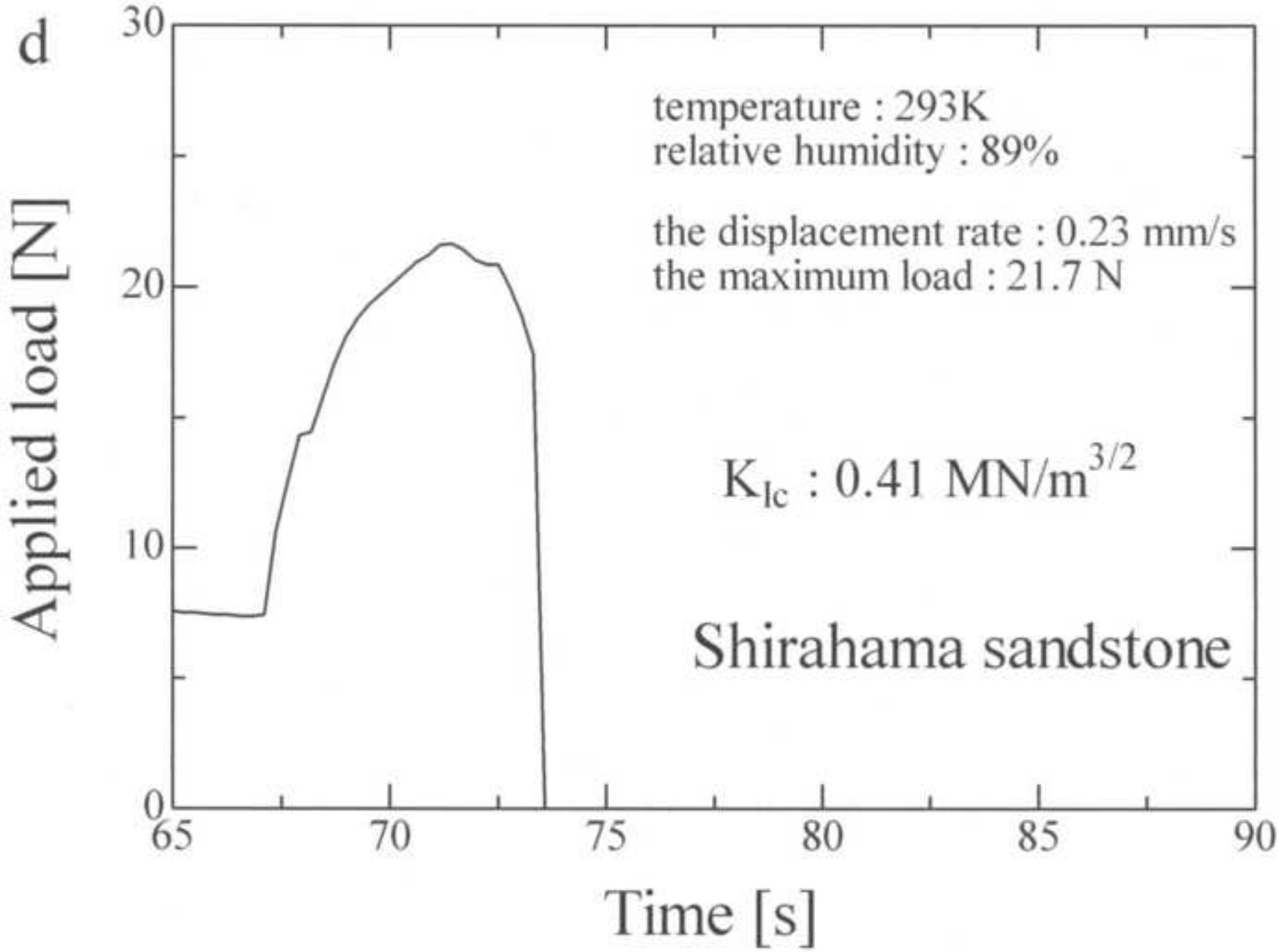

Figure3e
Click here to download high resolution image

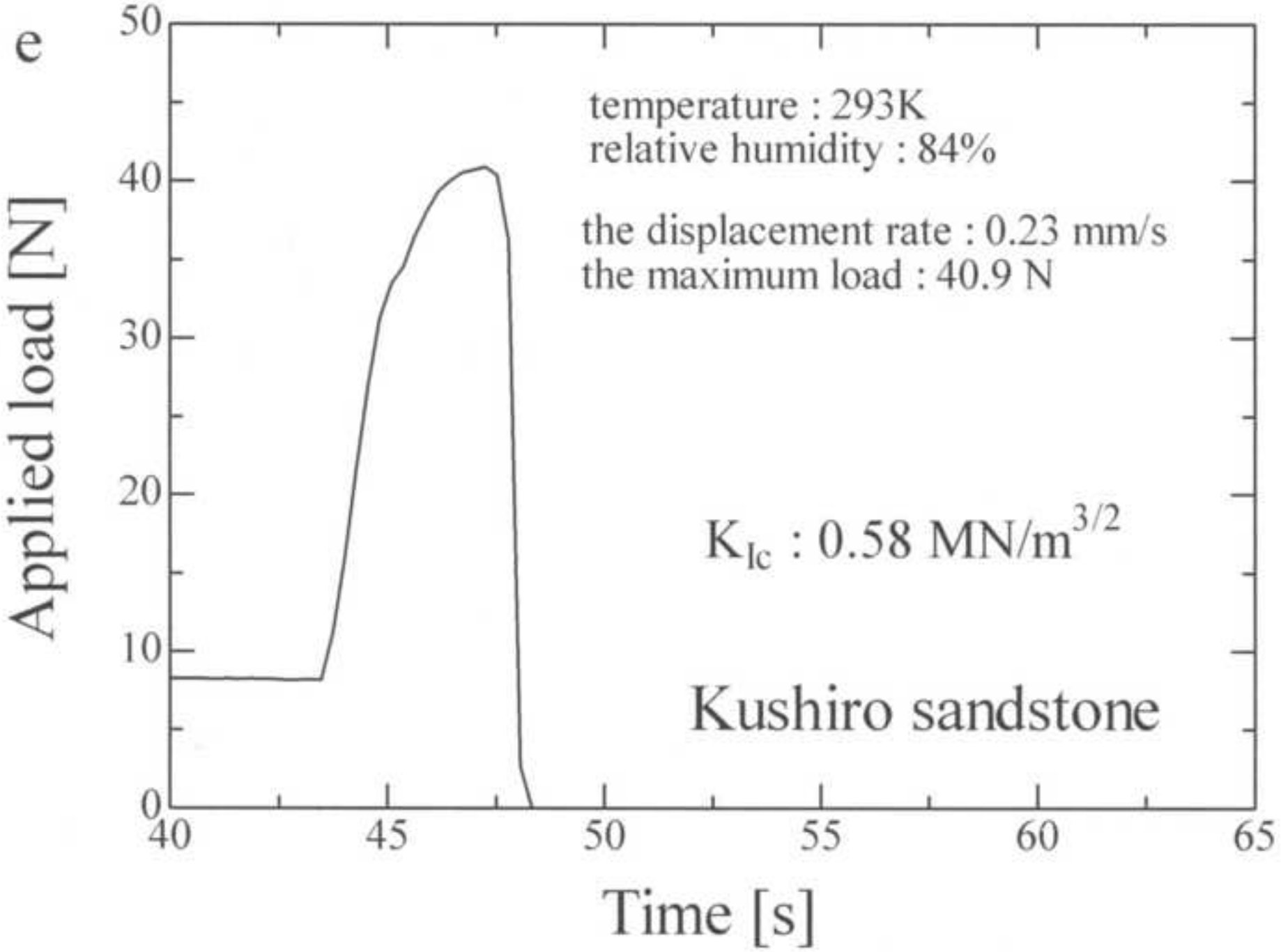

Figure4a
Click here to download high resolution image

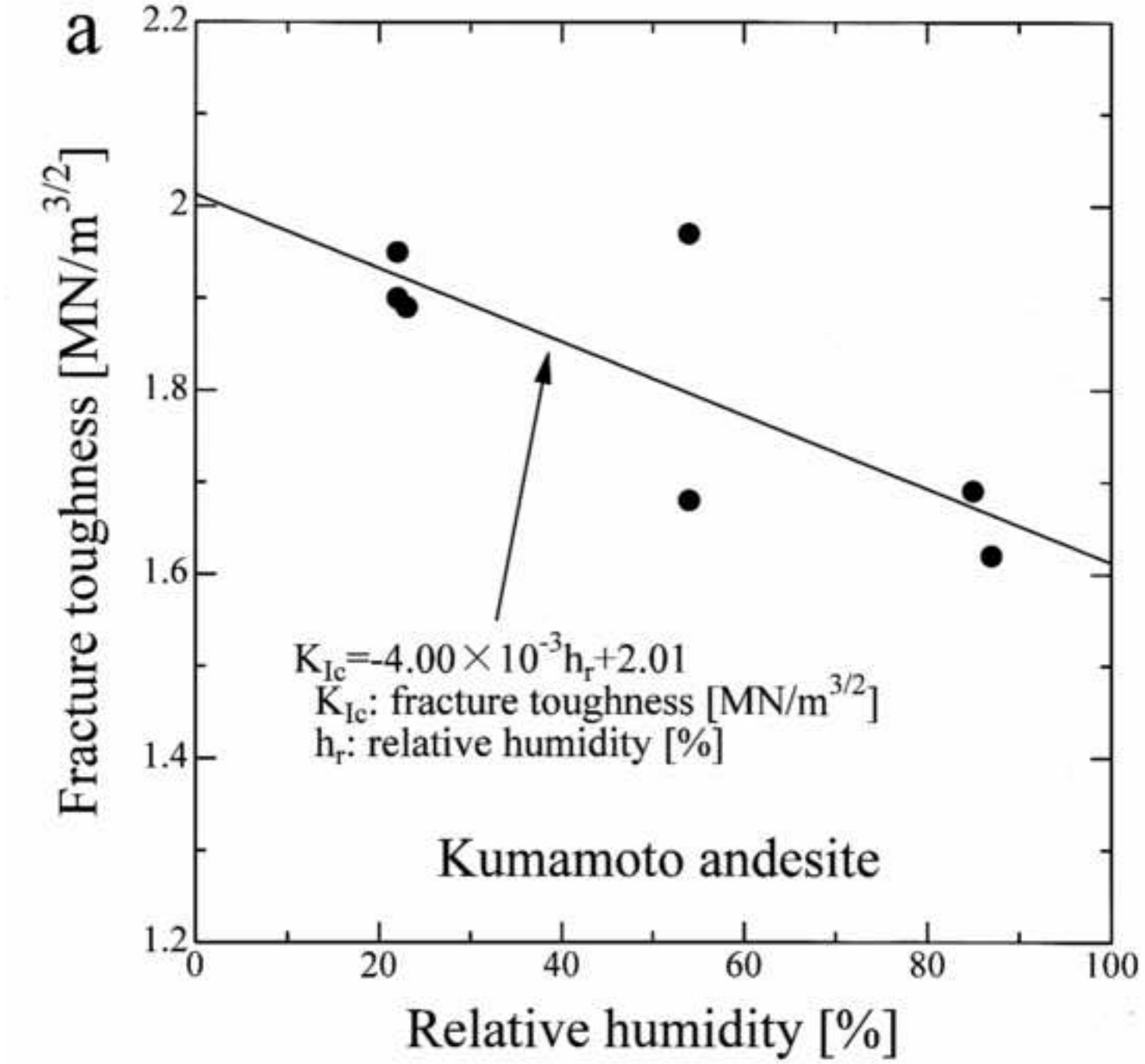

Figure4b

Click here to download high resolution image

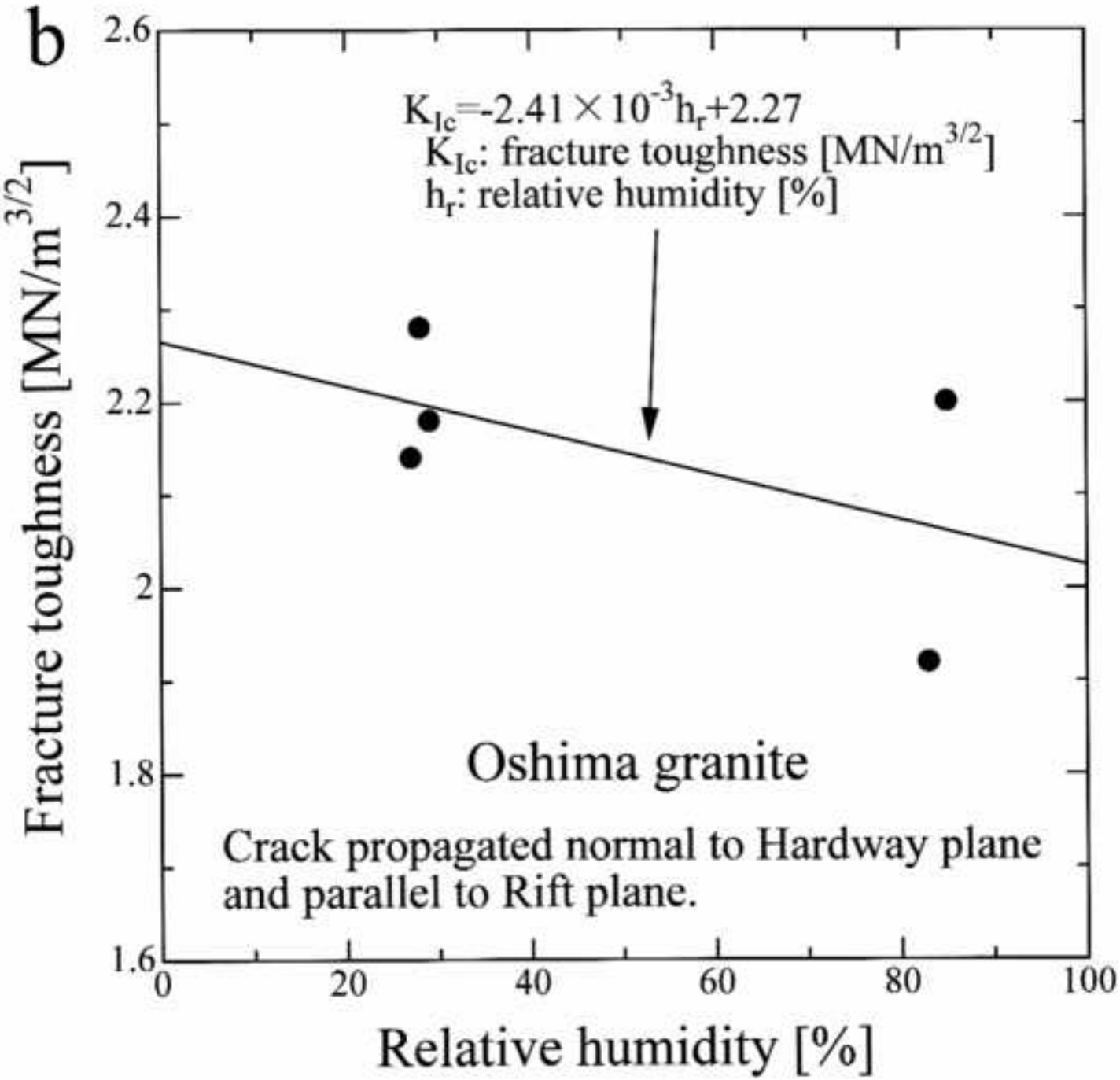

Figure4c
Click here to download high resolution image

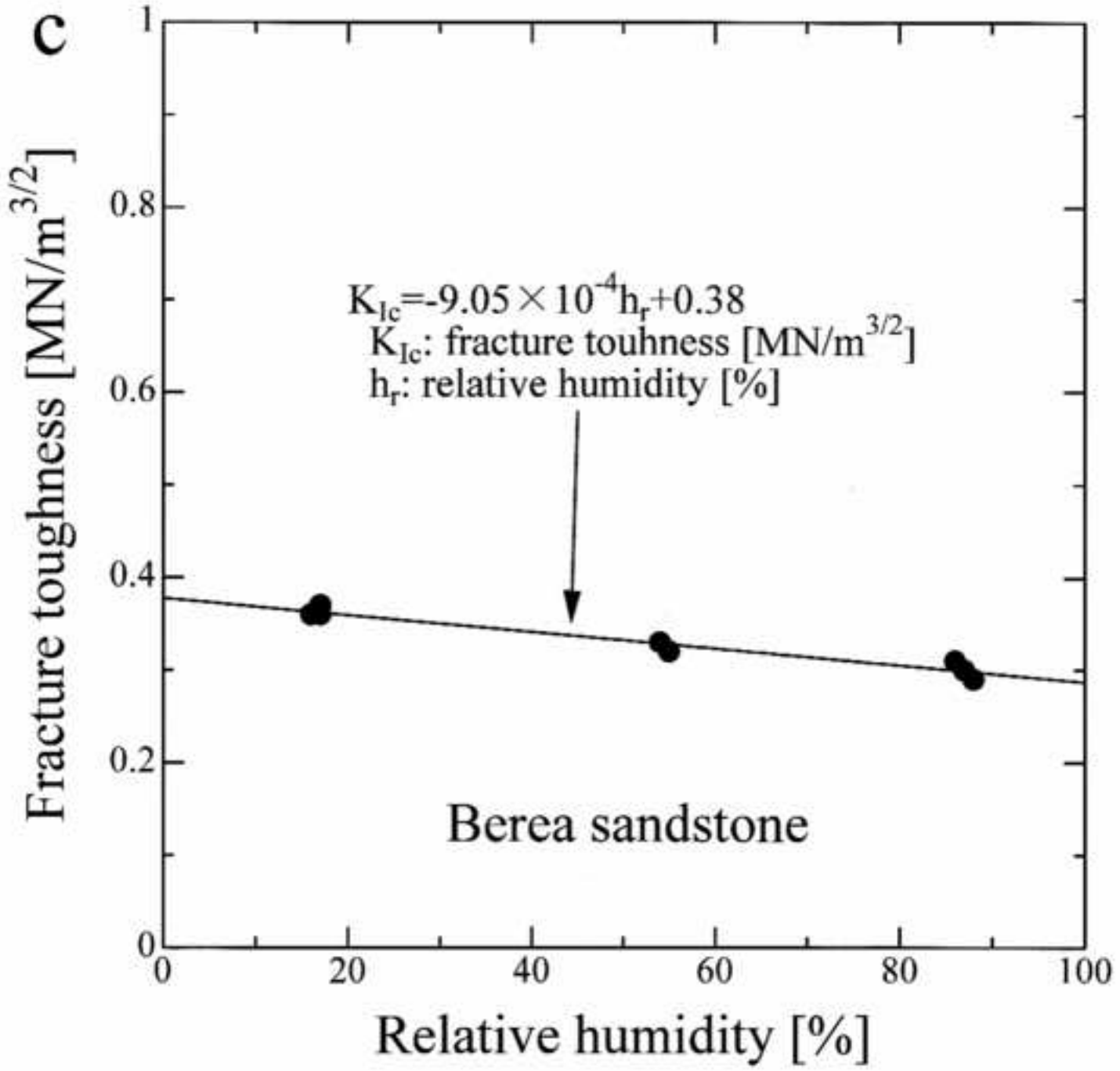

Figure4d

Click here to download high resolution image

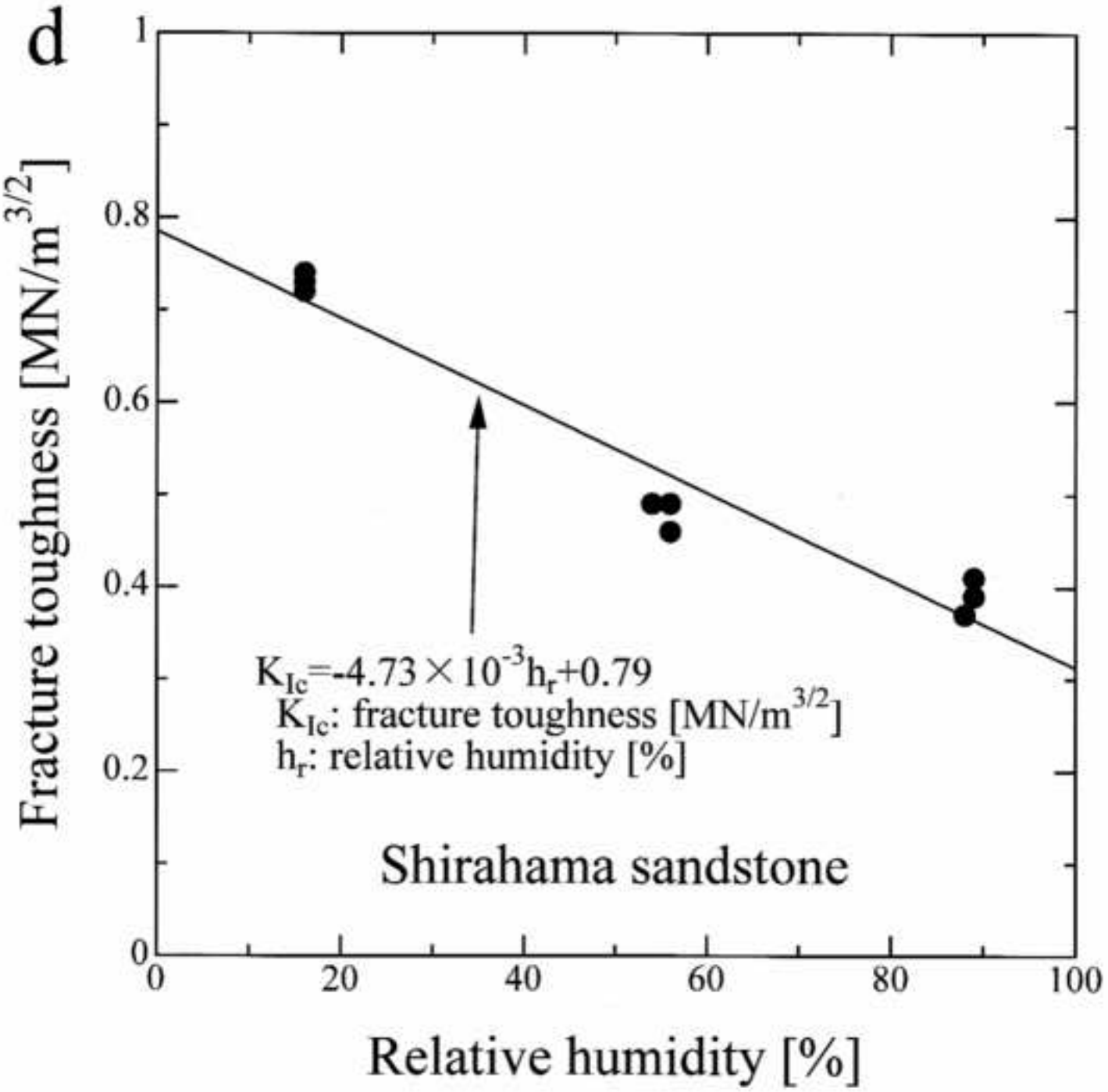

Figure4e

Click here to download high resolution image

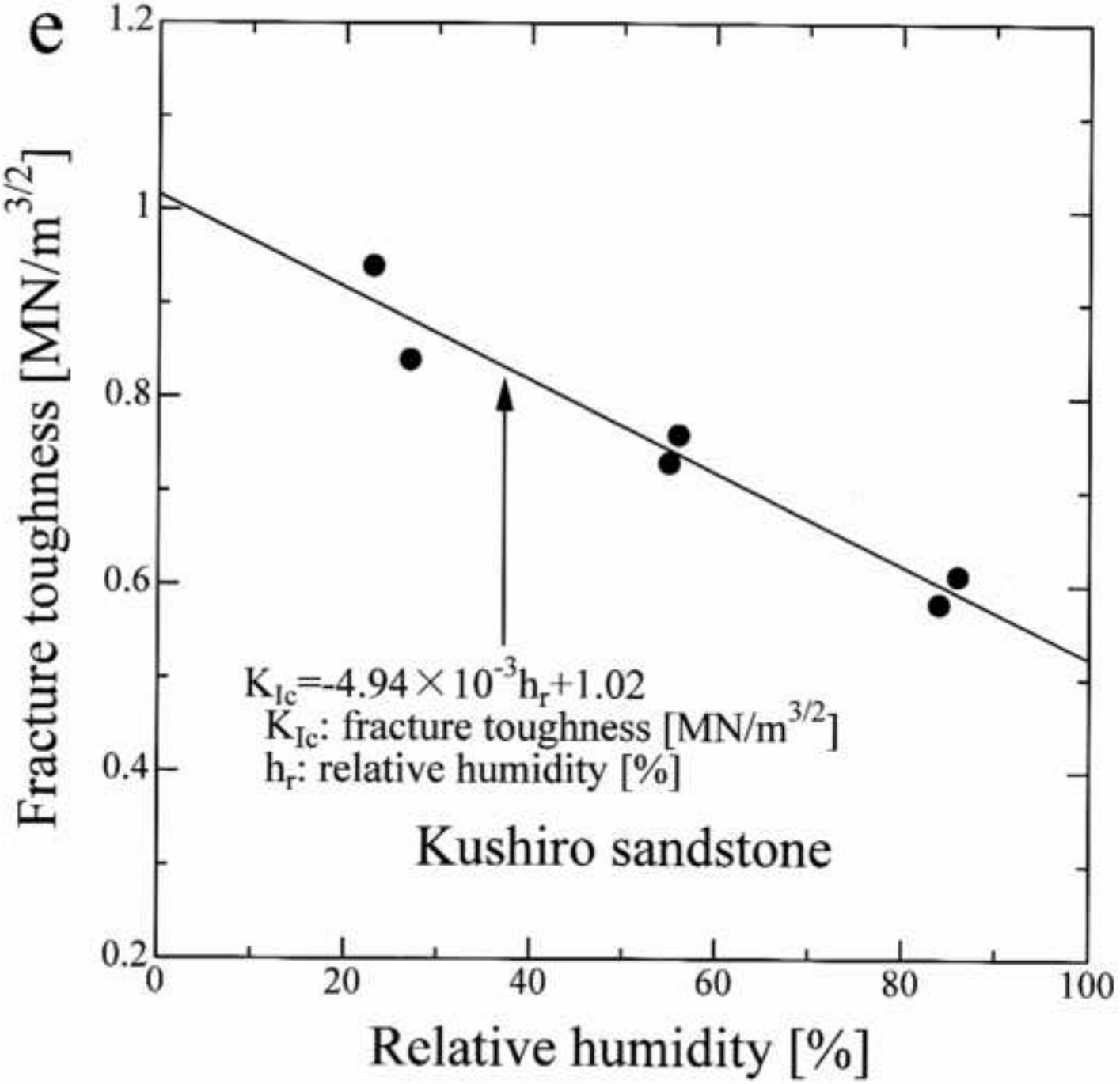

Figure5a

Click here to download high resolution image

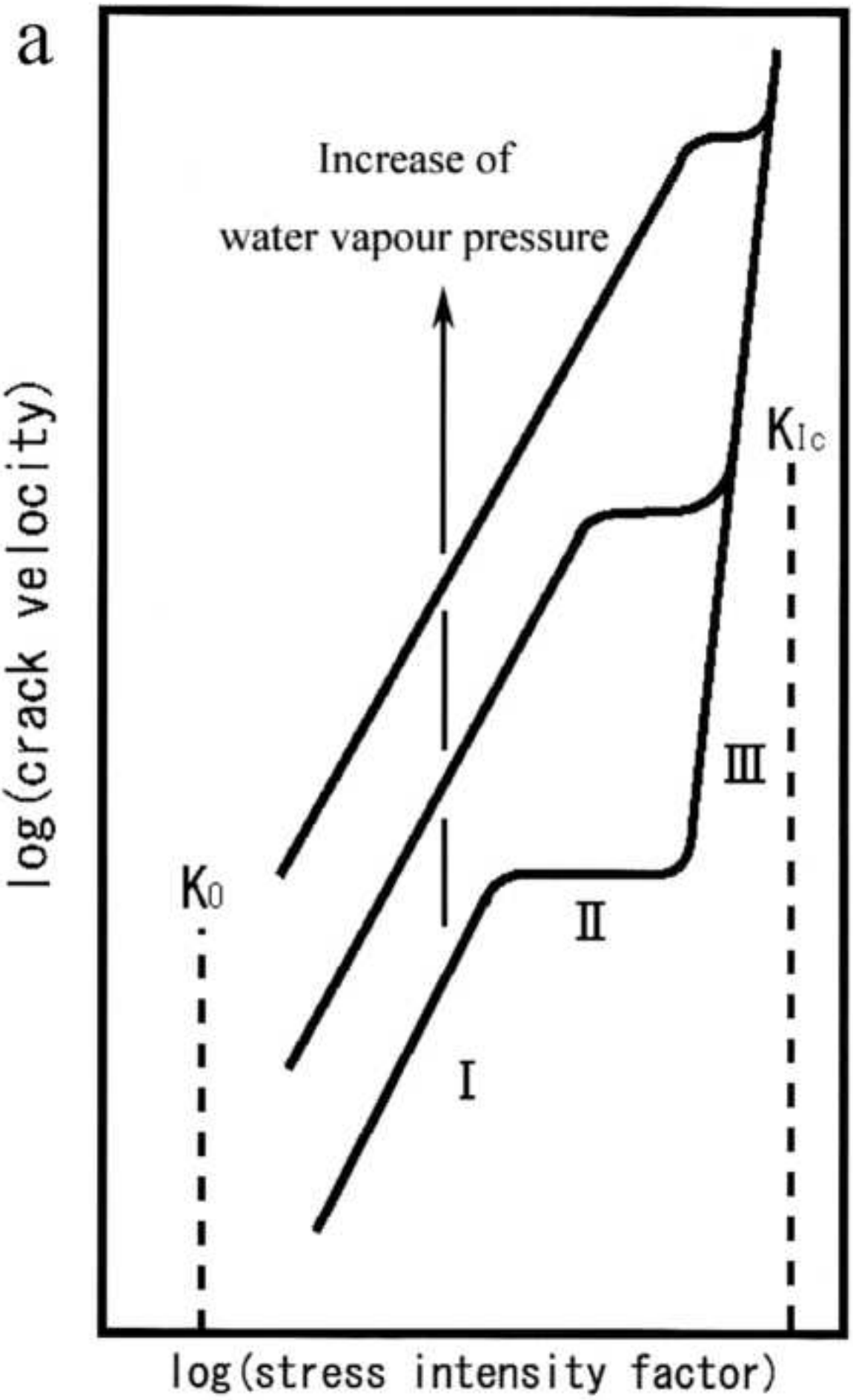

Figure5b

Click here to download high resolution image

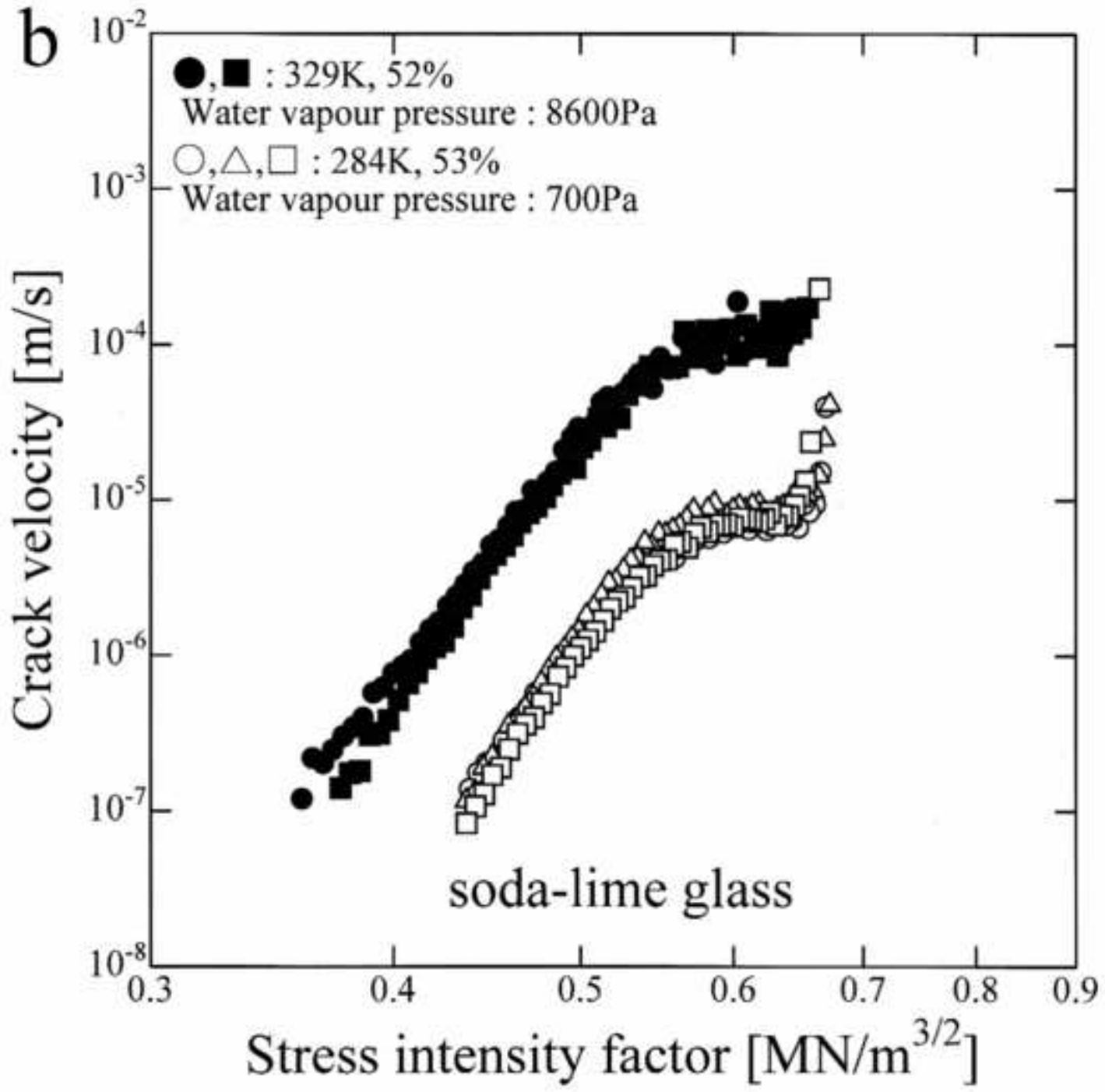

Figure6

Click here to download high resolution image

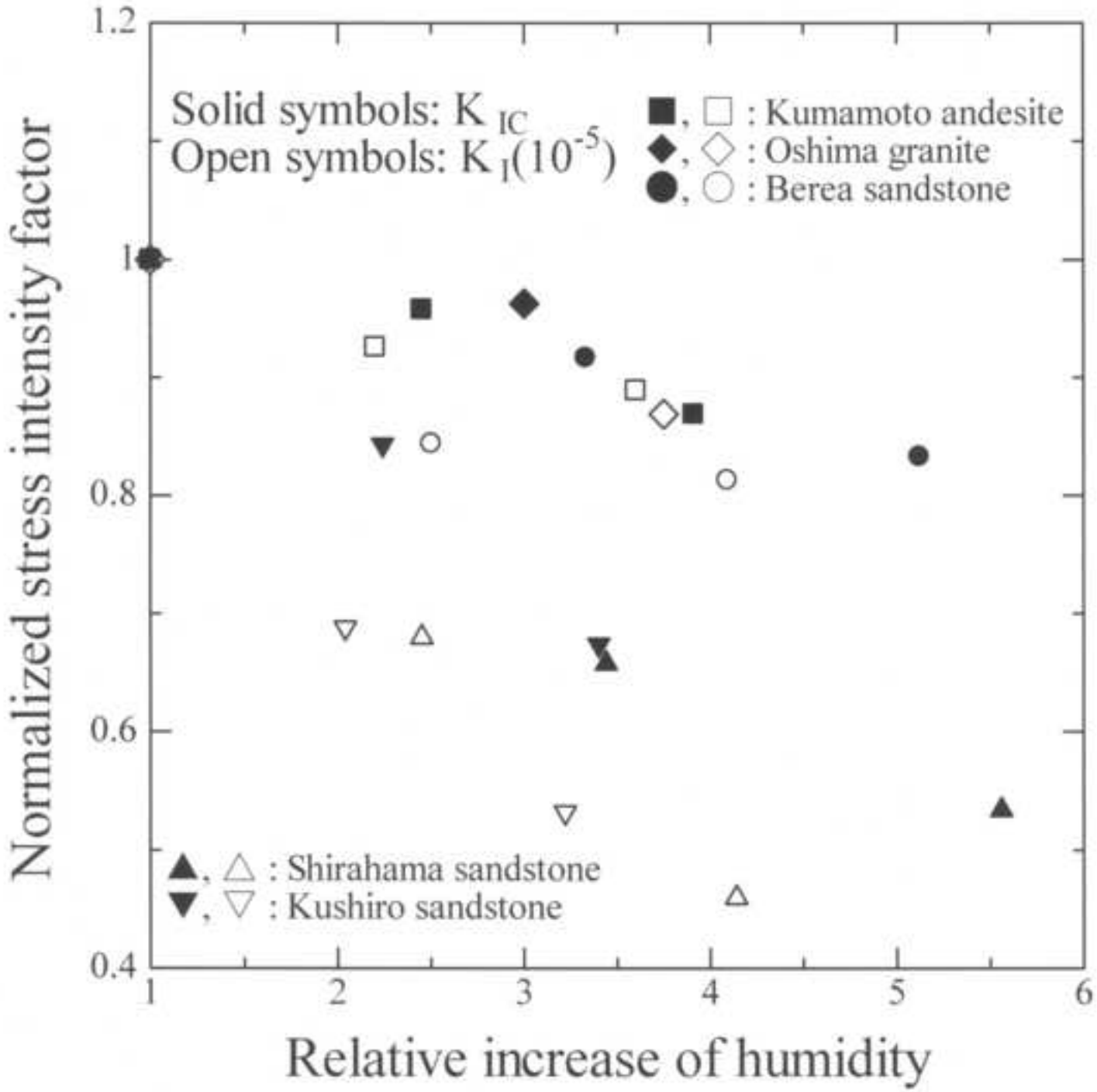

Figure7a

Click here to download high resolution image

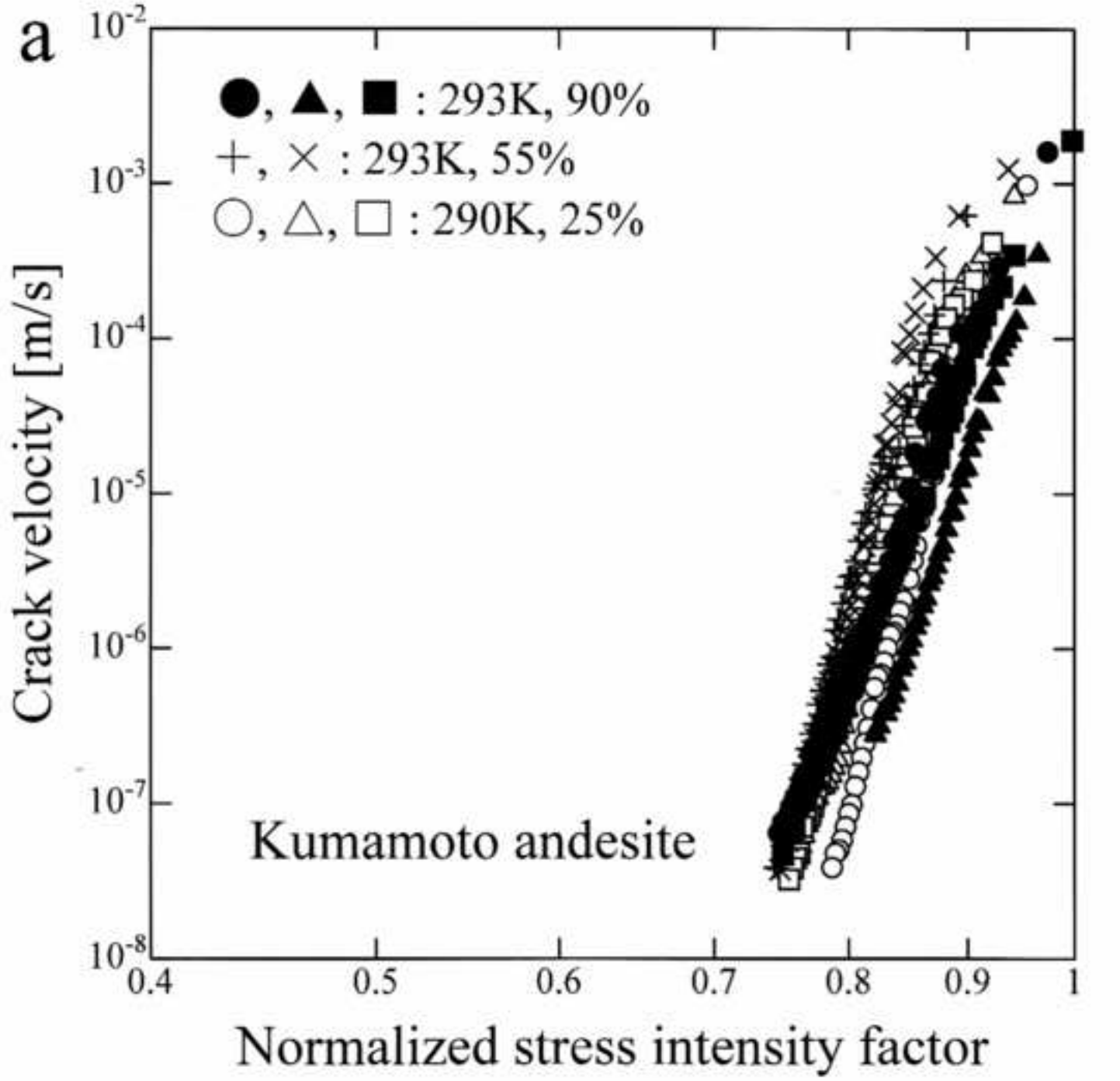

Figure7b

Click here to download high resolution image

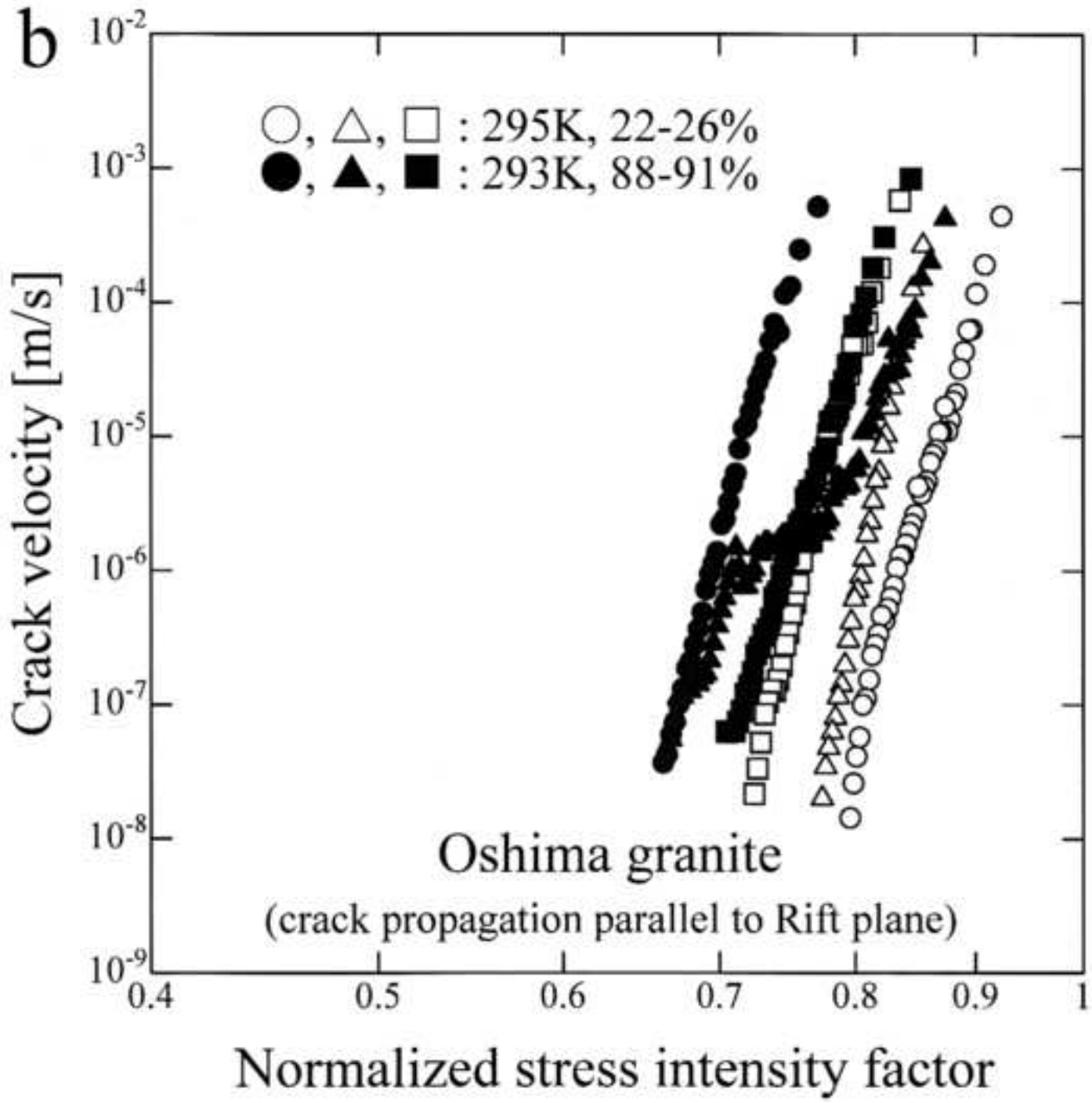

Figure7c
Click here to download high resolution image

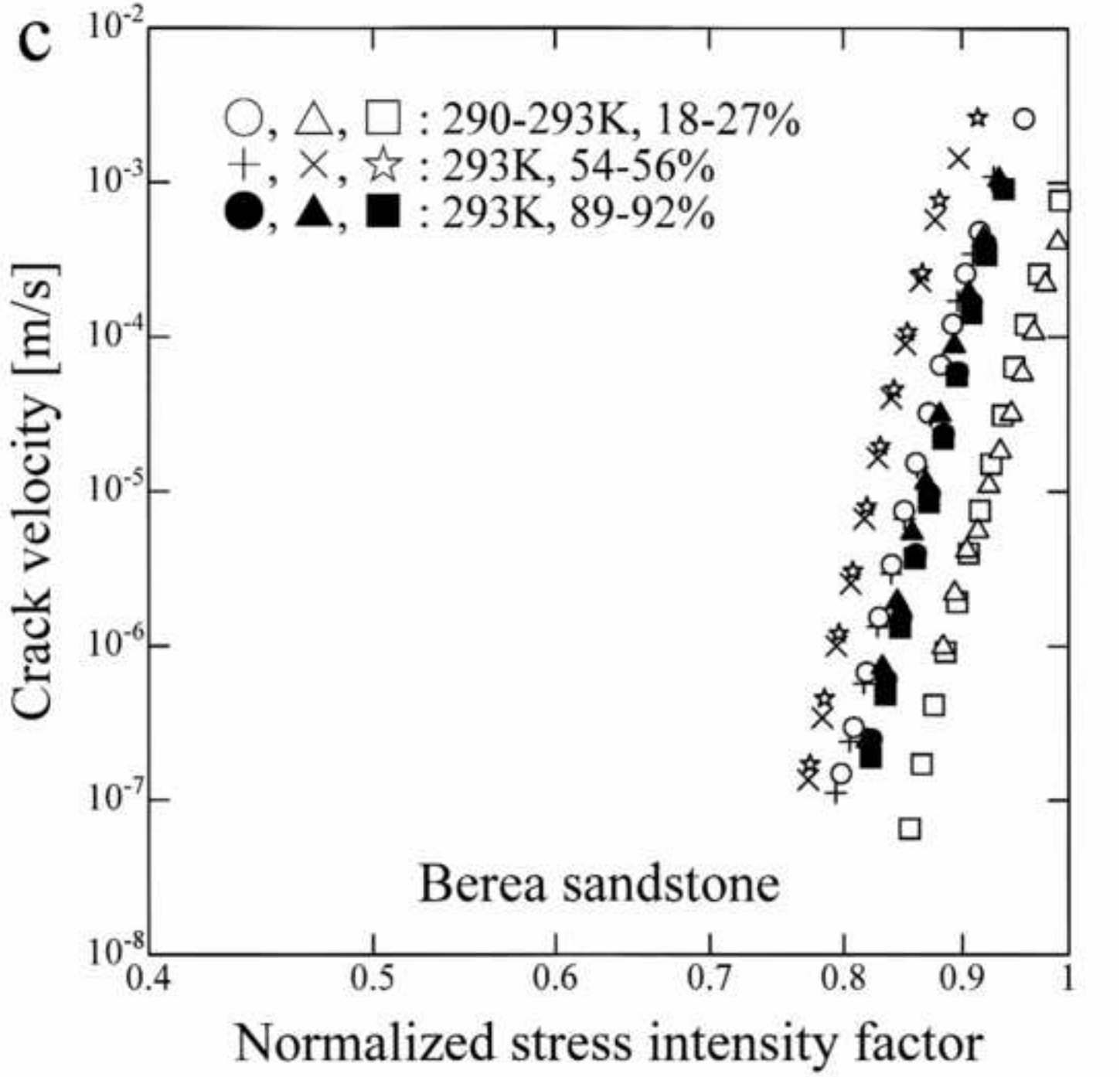

Figure7d
Click here to download high resolution image

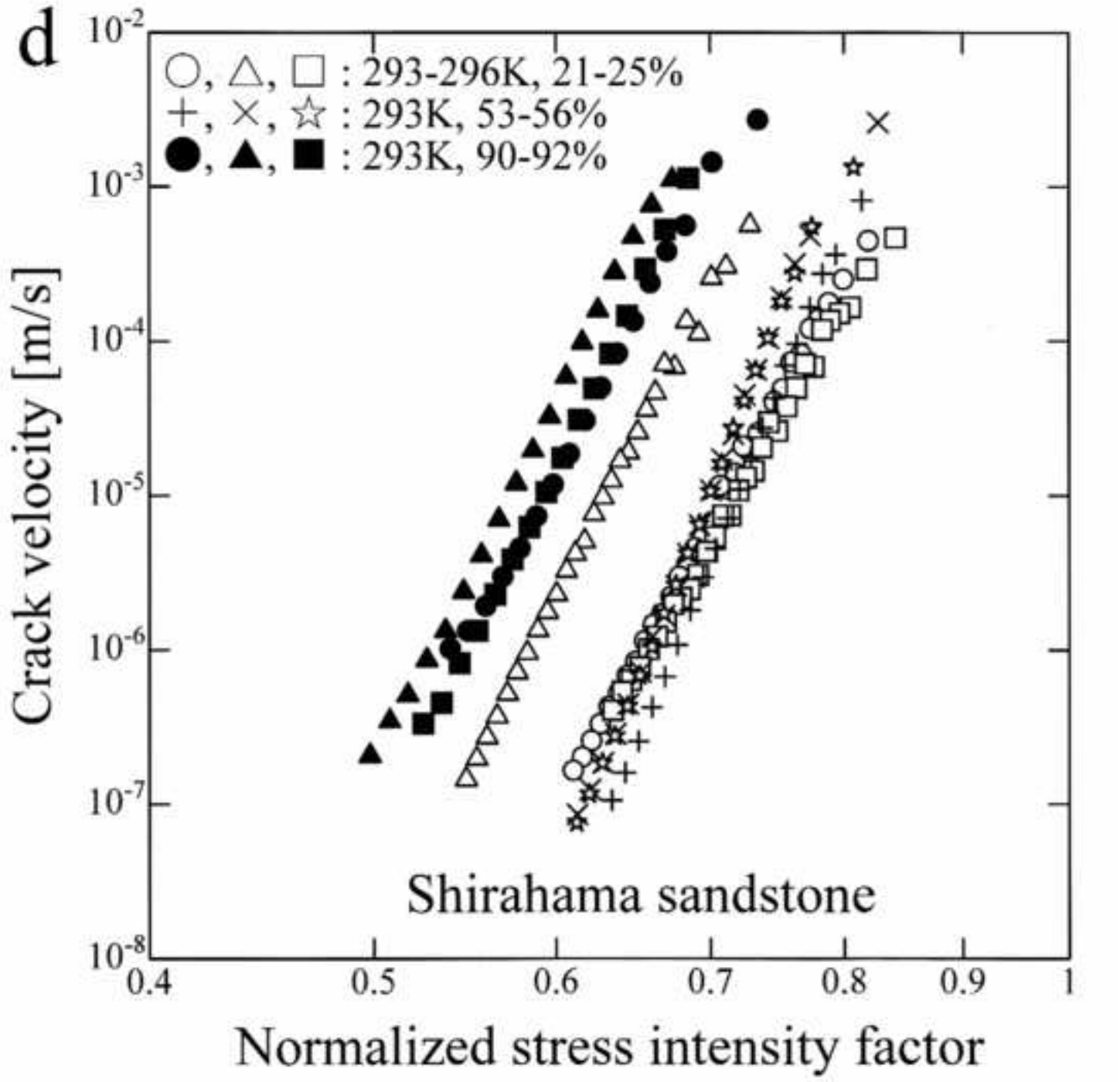

Figure7e
Click here to download high resolution image